Mass Spectrometric Fingerprints of Organic Compounds in NaCl-Rich Ice Grains from Europa and Enceladus

Maryse Napoleoni[1]*, *Fabian Klenner*[1], *Nozair Khawaja*[1], *Jon K. Hillier*[1], *Frank Postberg*[1]

[1]Institute of Geological Sciences, Freie Universität Berlin, Berlin 12249, Germany

*corresponding author: m.napoleoni@fu-berlin.de

Supplementary Information

Additional Methods

The principle of delayed extraction in the LILBID setup

The Time-of-Flight (TOF) mass spectrometer uses the principle of delayed extraction[1] (Figure 1). Ions cross a field-free drift region before reaching the acceleration (or extraction) region. When the acceleration electrodes (repeller and extractor) are switched on (after a predefined delay time), fast ions have already crossed more of the acceleration region than slow ions, so they experience a weaker electrical field than slow ions. Ions within a defined range of initial velocities can thus be selected for analysis by adjusting the delay time. Ions arriving later than the delay time are blocked by the repeller applying a potential that prevents them to enter the mass spectrometer detector. The delay time is therefore defined as the time between the laser shot (T_0) and the ion acceleration. Selecting a range of ion velocities allows the selection of ions of a specific range of masses, since ion velocities are related to their masses and the amount of energy imparted by the laser (i.e., $v \sim \sqrt{\frac{E_{laser}}{m}}$). The conversion from TOF to m/z is performed using a second order calibration equation [2]. This mass calibration is done with the LabView software on the measurement computer. The spectra are recalibrated to reduce possible mass shifts [3] (i.e., deviances up to >1 u due to the delayed extraction method and variable initial ion velocities) with a Python script that calculates a polynomial function based on real peak masses and assigns the corresponding data file with this function.

Supplementary references

(1) Klenner, F.; Postberg, F.; Hillier, J.; Khawaja, N.; Reviol, R.; Srama, R.; Abel, B.; Stolz, F.; Kempf, S. Analogue Spectra for Impact Ionization Mass Spectra of Water Ice Grains Obtained at Different Impact Speeds in Space. *Rapid Commun Mass Spectrom* **2019**, *33* (22), 1751–1760. https://doi.org/10.1002/rcm.8518

(2) Klenner, F.; Umair, M.; Walter, S. H. G.; Khawaja, N.; Hillier, J.; Nölle, L.; Zou, Z.; Napoleoni, M.; Sanderink, A.; Zuschneid, W.; Abel, B.; Postberg, F. Developing a Laser Induced Liquid Beam Ion Desorption Spectral Database as Reference for Spaceborne Mass Spectrometers. *Earth and Space Science* **2022**, *9* (9). https://doi.org/10.1029/2022EA002313

(3) Christian, N. P.; Arnold, R. J.; Reilly, J. P. Improved Calibration of Time-of-Flight Mass Spectra by Simplex Optimization of Electrostatic Ion Calculations. *Anal. Chem.* **2000**, *72* (14), 3327–3337. https://doi.org/10.1021/ac991500h

Additional Figures

The spectra of solutions not included in this work, i.e. anion mass spectrum of 5-amino-1-pentanol in 1M NaCl matrix, cation mass spectrum of benzoic acid in 1M NaCl, anion mass spectrum of butylamine in 1M NaCl, anion mass spectrum of glucose in 1M NaCl, anion mass spectrum of methanol in 1M NaCl matrix, and the anion mass spectra of pyridine in 0.1M and 1M NaCl matrix showed no peak related to the organics and are similar to the respective NaCl background matrix spectra (Figures 2,3,S1-S4). In the spectra of organics in salt-rich matrices (figure S5 to S36), unlabeled peaks originate exclusively from the salty matrix.

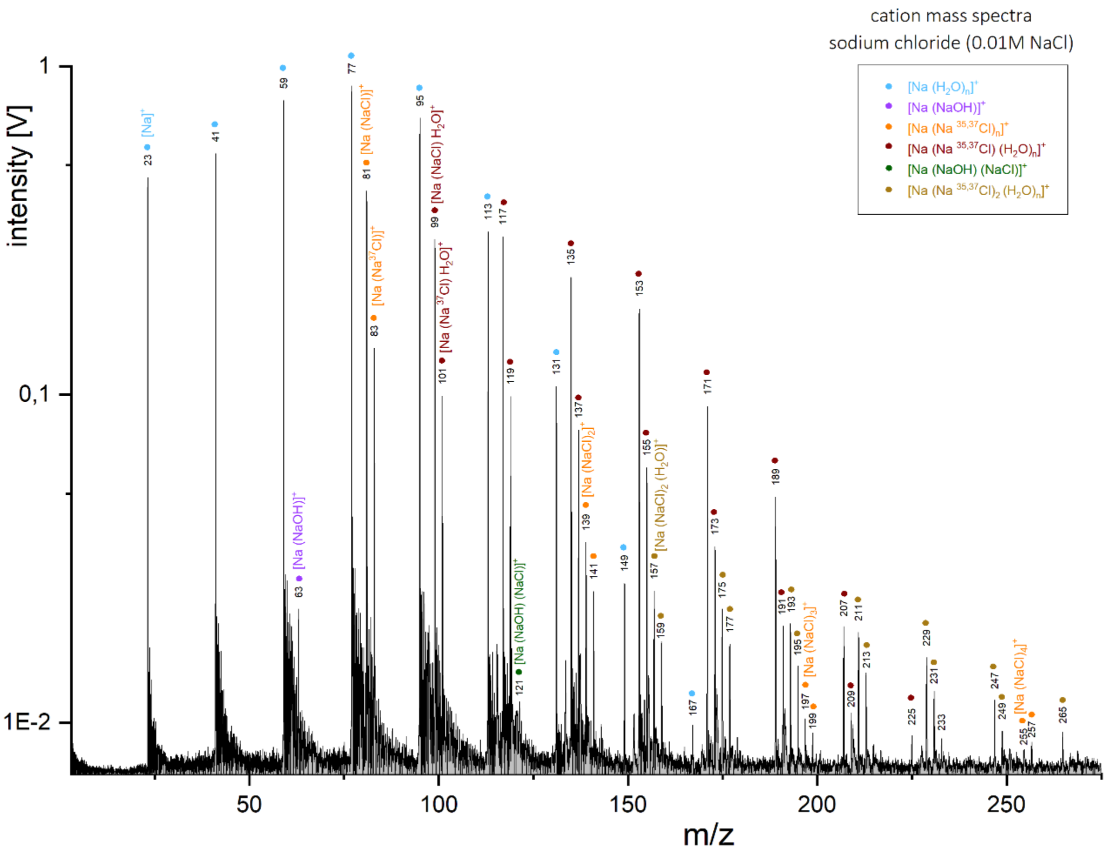

Figure S1. Baseline corrected cation mass spectrum of sodium chloride (NaCl) at a concentration of 0.01M, recorded at a delay time of 6.2µs.

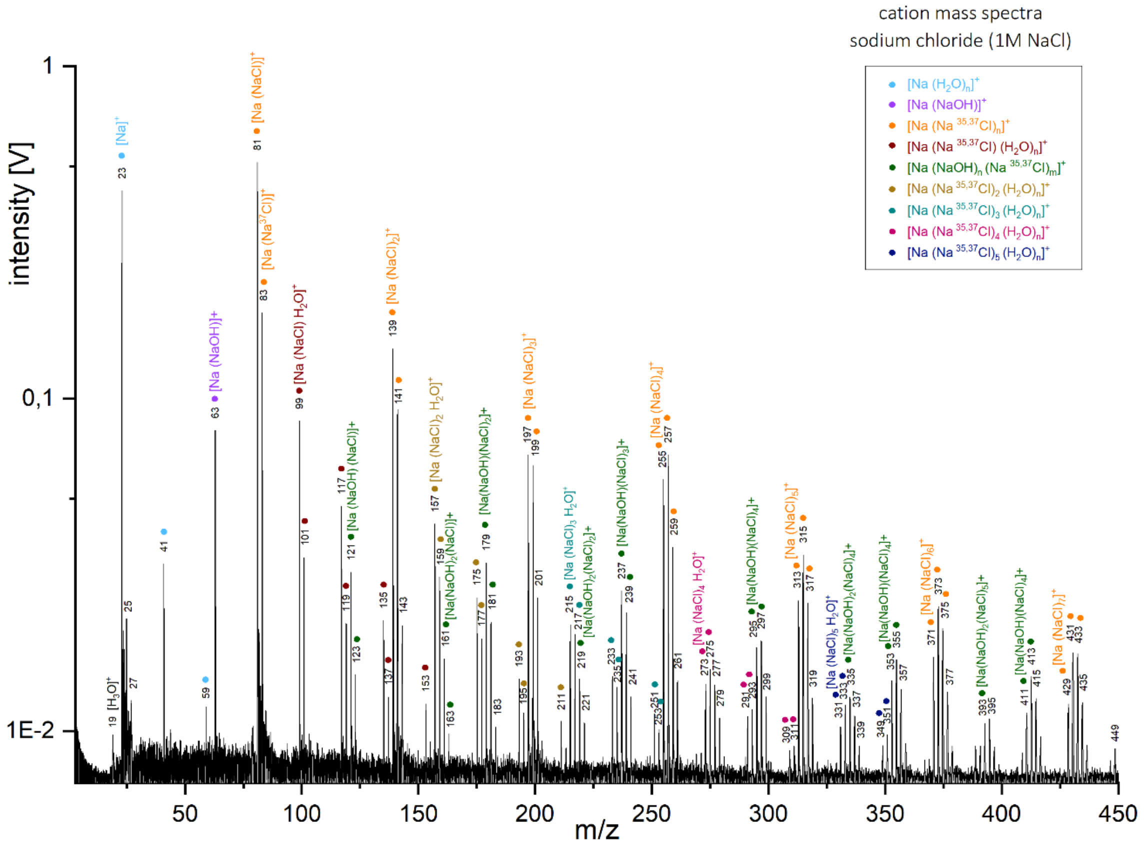

Figure S2. Baseline corrected cation mass spectrum of sodium chloride (NaCl) at a concentration of 1M, recorded at a delay time of 6.2µs.

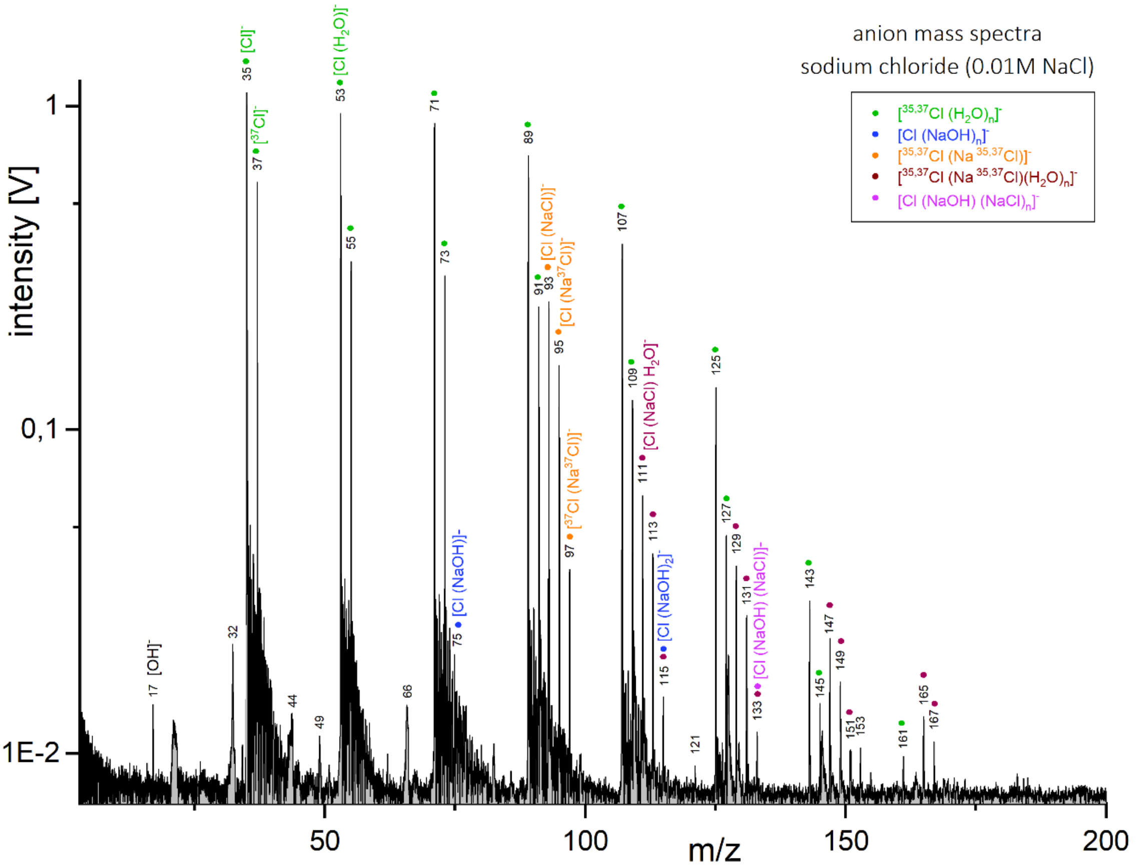

Figure S3. Baseline corrected anion mass spectrum of sodium chloride (NaCl) at a concentration of 0.01M, recorded at a delay time of 6.1µs.

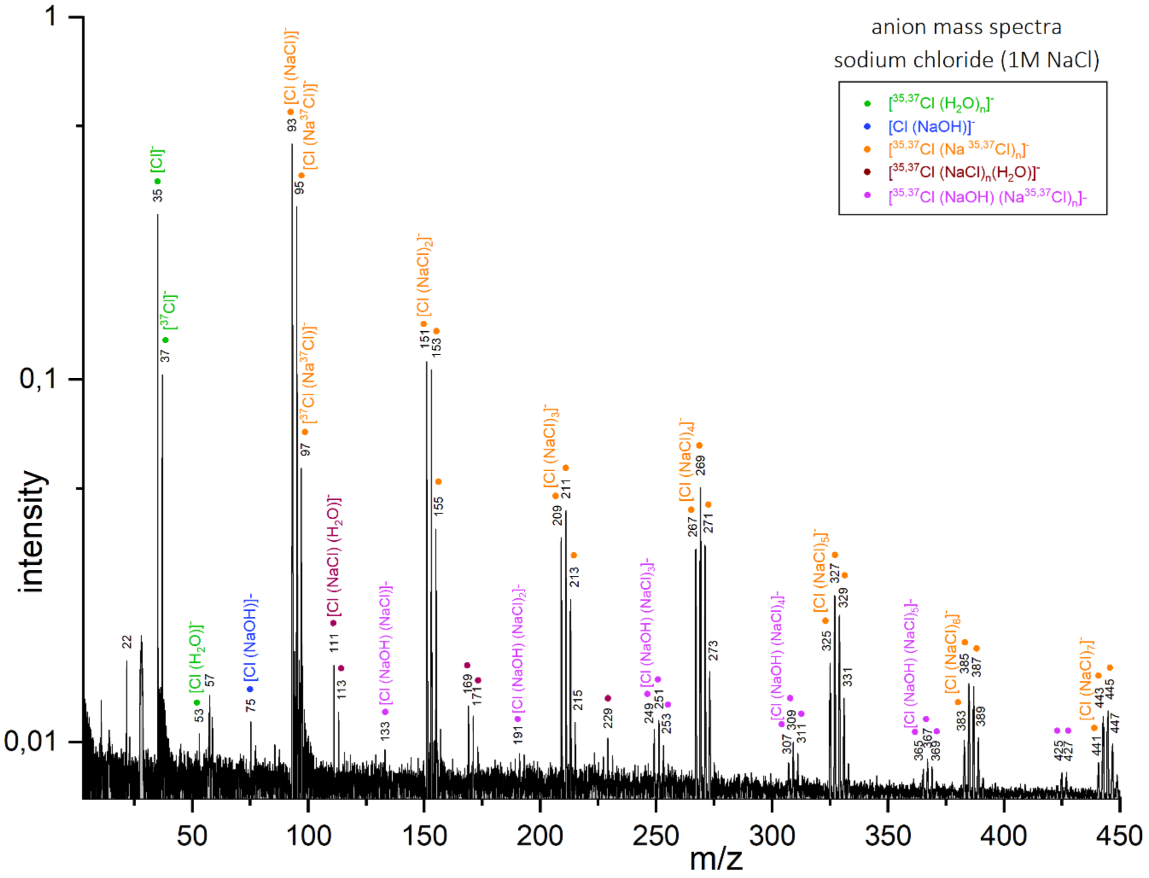

Figure S4. Baseline corrected anion mass spectrum of sodium chloride (NaCl) at a concentration of 1M, recorded at a delay time of 6.2µs.

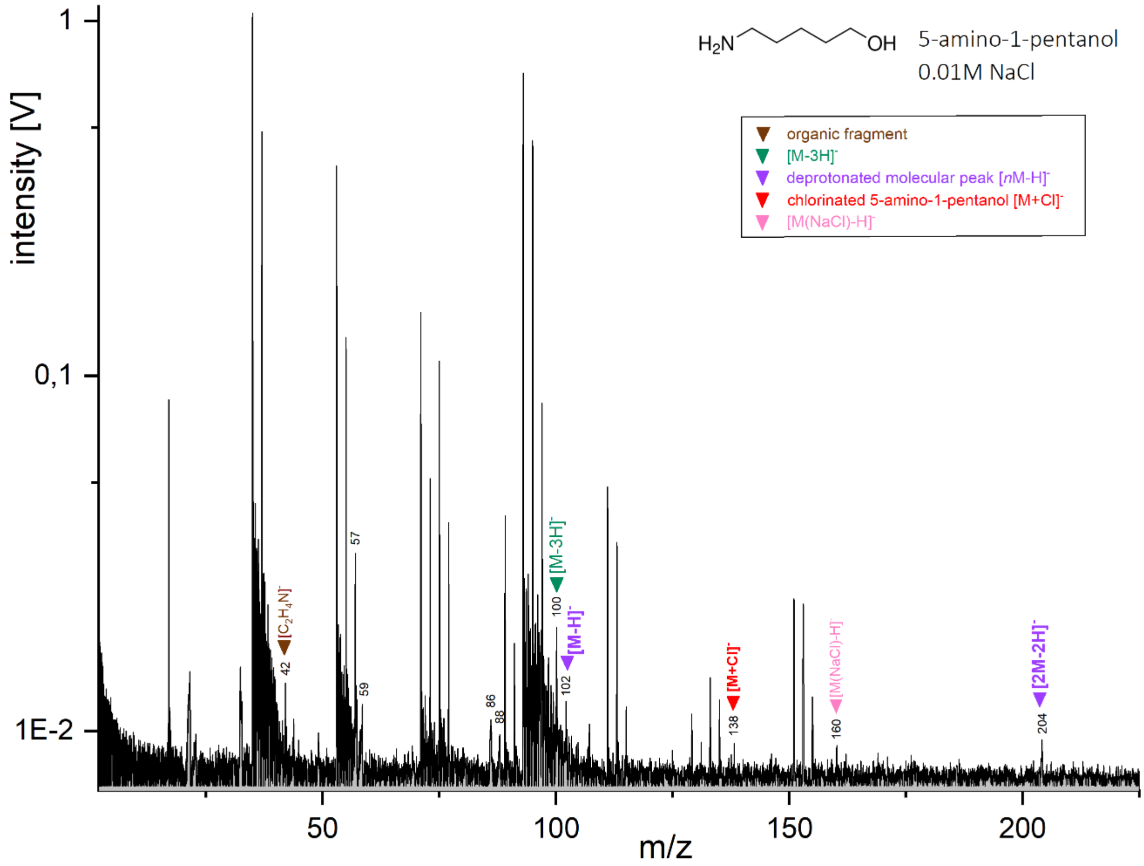

Figure S5. Baseline corrected anion mass spectrum of 5-amino-1-pentanol at a concentration of 5wt% in a H_2O and NaCl (0.01M) matrix, recorded at a delay time of 5.5µs.

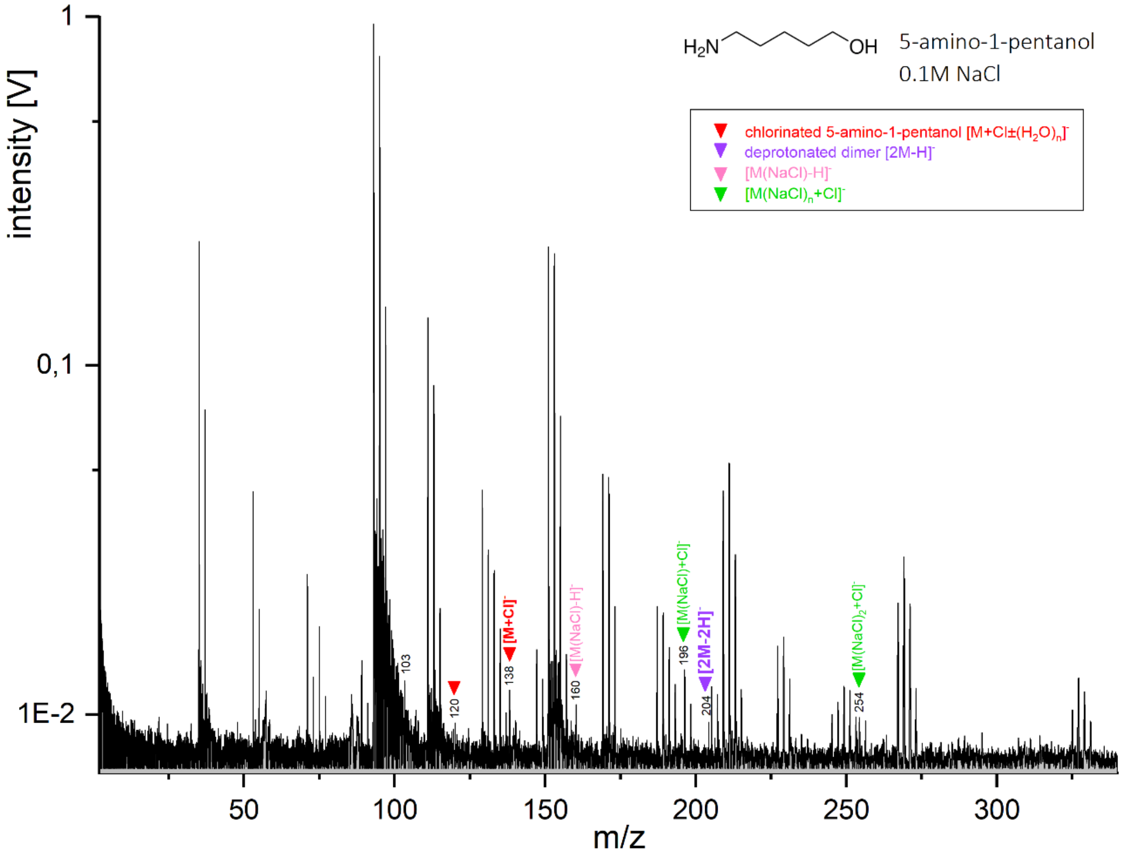

Figure S6. Baseline corrected anion mass spectrum of 5-amino-1-pentanol at a concentration of 5wt% in a H_2O and NaCl (0.1M) matrix, recorded at a delay time of 6.2µs.

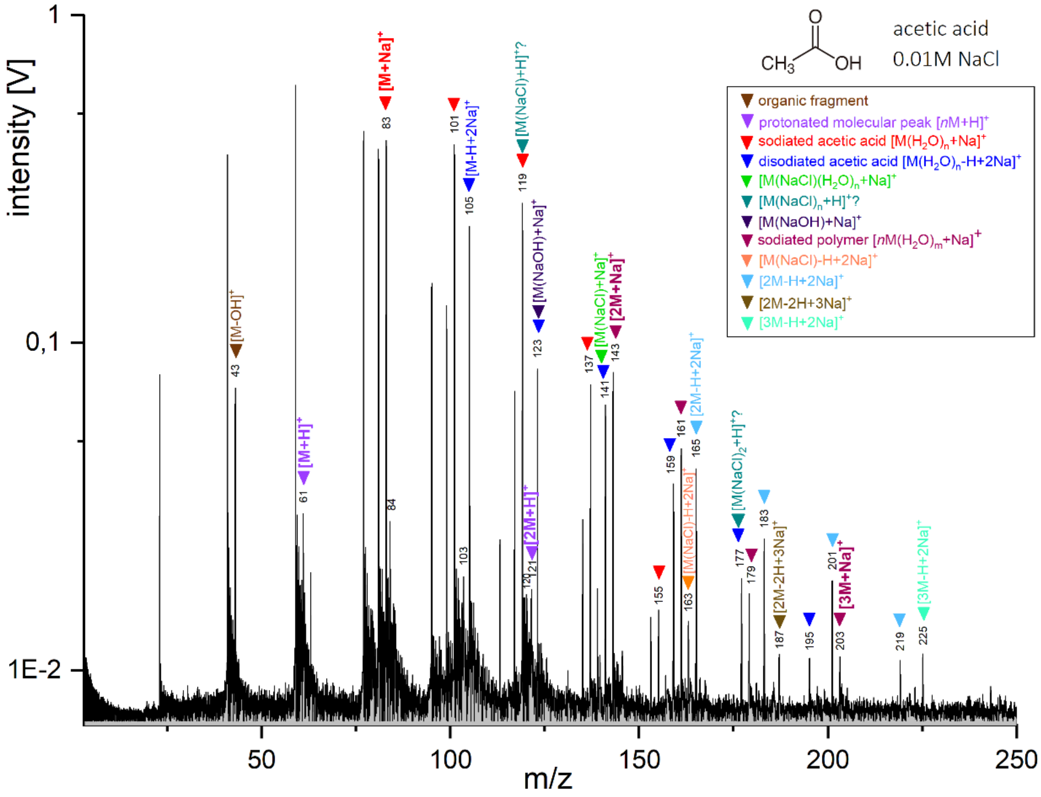

Figure S7. Baseline corrected cation mass spectrum of acetic acid at a concentration of 5wt% in a H_2O and NaCl (0.01M) matrix, recorded at a delay time of 6.0µs. The peak at m/z 83u (0.416 V) is assigned to both the salt cluster $[Na(Na^{37}Cl)]^+$ (0.125V) and sodiated acetic acid $[M+Na]^+$ (0.291 V). Peaks at m/z 123u and 141u have been tentatively assigned to acetic acid and salt clusters $[M+Na+NaOH]^+$ and $[M+Na+NaCl]^+$ but can also be water clusters of disodiated acetic acid.

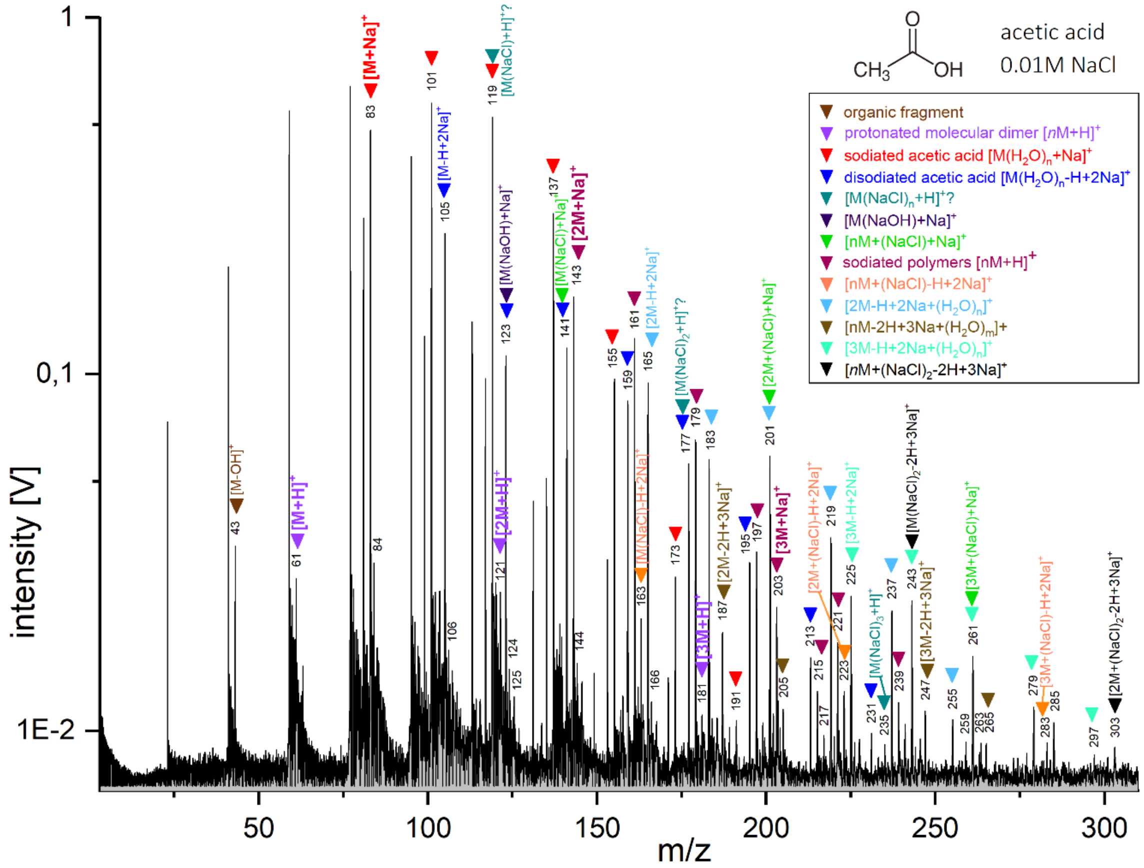

Figure S8. Baseline corrected cation mass spectrum of acetic acid at a concentration of 5wt% in a H_2O and NaCl (0.01M) matrix, recorded at a delay time of 6.5µs. Unlabeled peaks originate exclusively from the salty matrix.

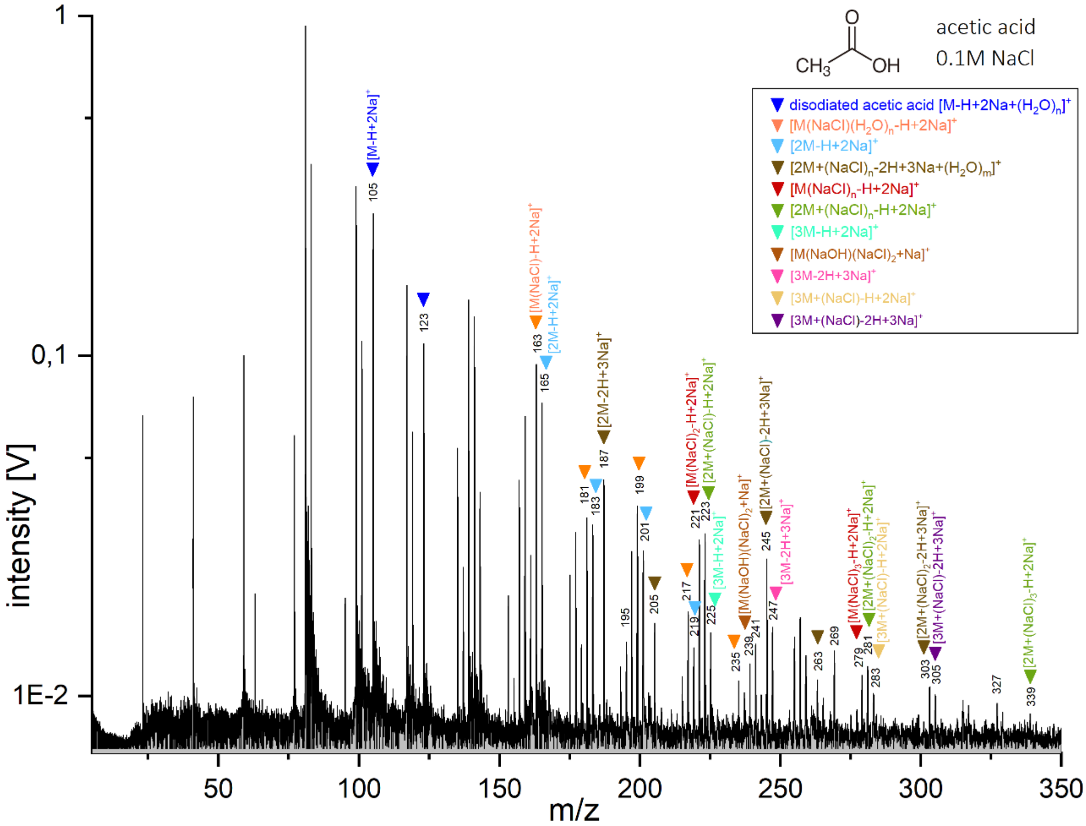

Figure S9. Baseline corrected cation mass spectrum of acetic acid at a concentration of 5wt% in a H_2O and NaCl (0.1M) matrix, recorded at a delay time of 6.0µs.

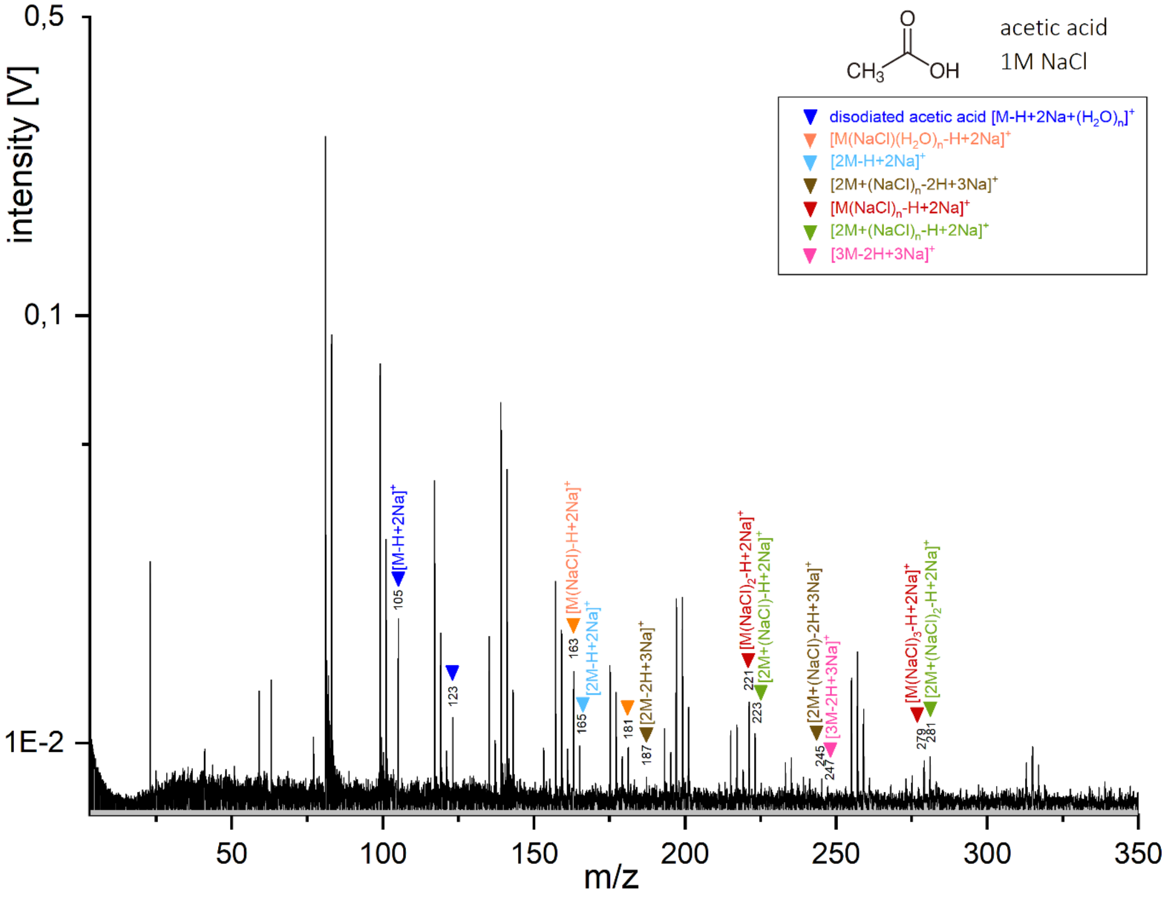

Figure S10. Baseline corrected cation mass spectrum of acetic acid at a concentration of 5wt% in a H_2O and NaCl (1M) matrix, recorded at a delay time of 6.0µs.

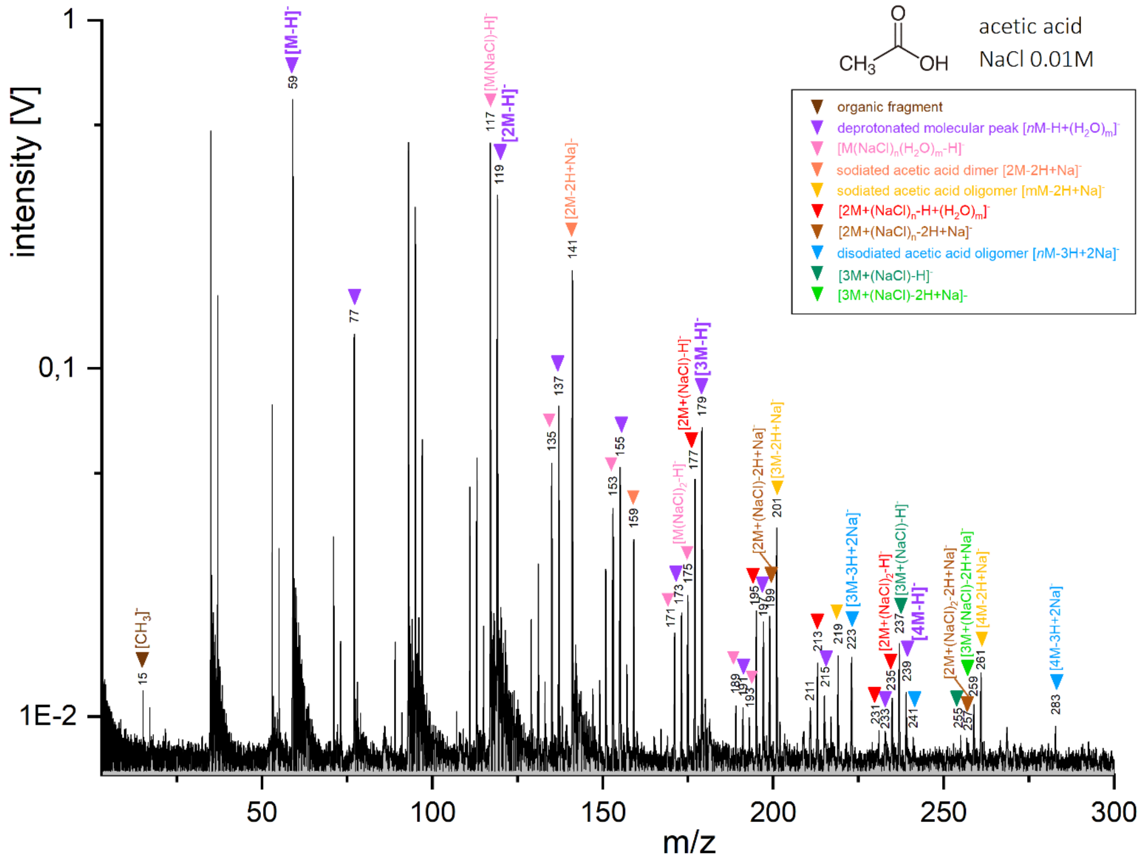

Figure S11. Baseline corrected anion mass spectrum of acetic acid at a concentration of 5wt% in a H_2O and NaCl (0.01M) matrix, recorded at a delay time of 6.5µs.

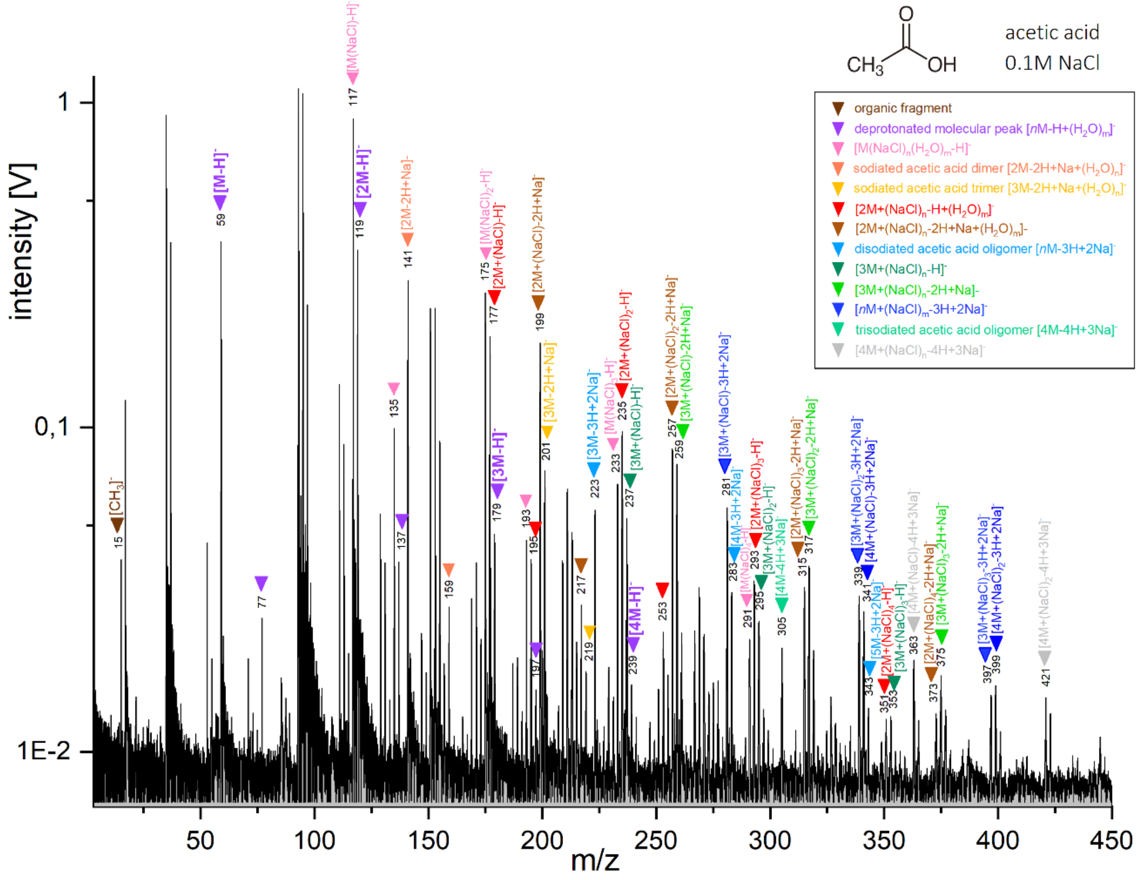

Figure S12. Baseline corrected anion mass spectrum of acetic acid at a concentration of 5wt% in a H_2O and NaCl (0.1M) matrix, recorded at a delay time of 6.5µs.

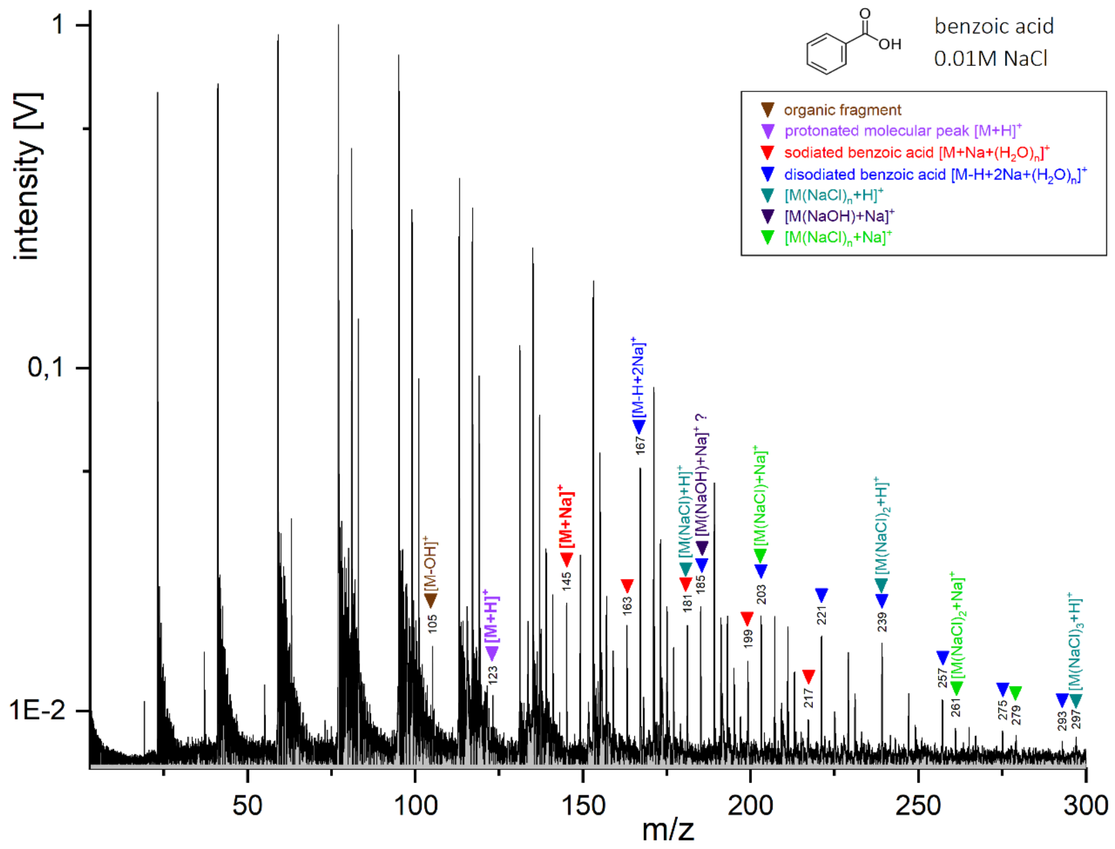

Figure S13. Baseline corrected cation mass spectrum of benzoic acid at a concentration of 0.17wt% in a H_2O and NaCl (0.01M) matrix, recorded at a delay time of 6.2µs.

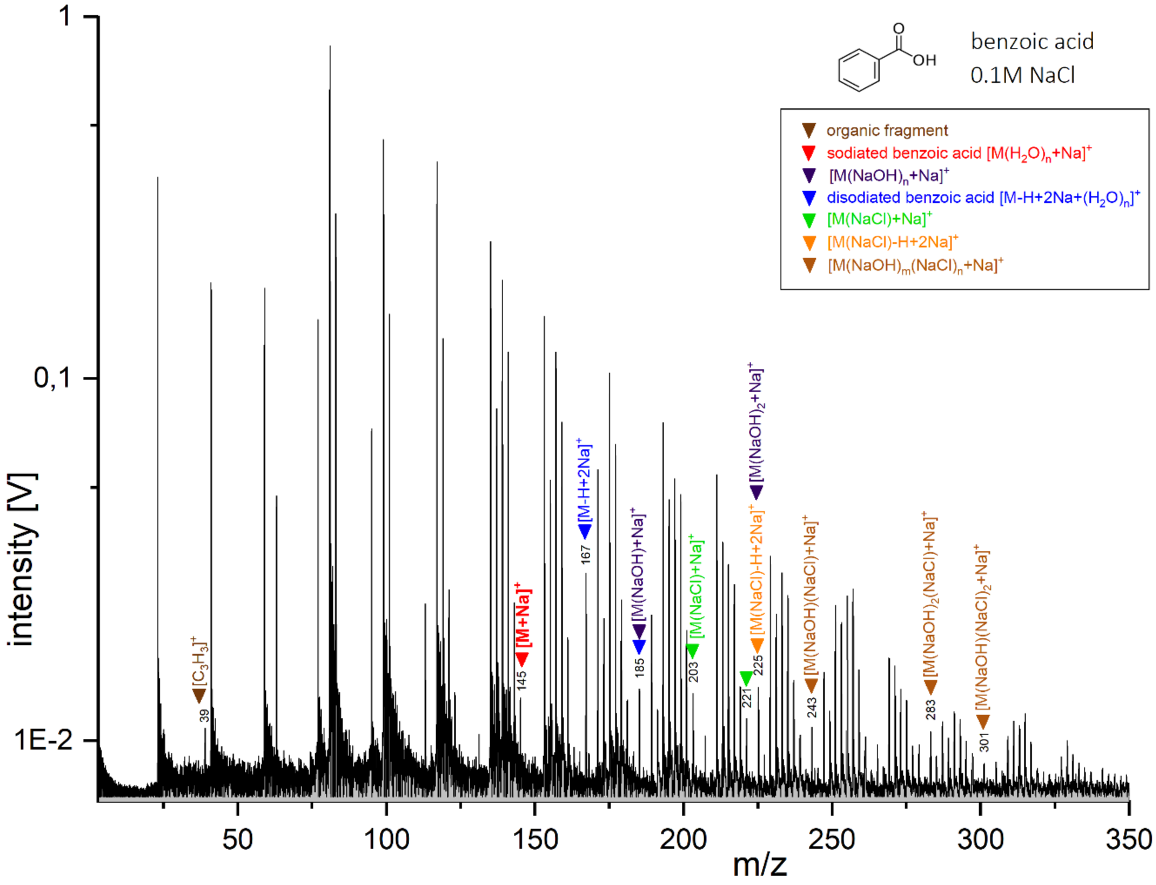

Figure S14. Baseline corrected cation mass spectrum of benzoic acid at a concentration of 0.17wt% in a H_2O and NaCl (0.1M) matrix, recorded at a delay time of 6.1µs.

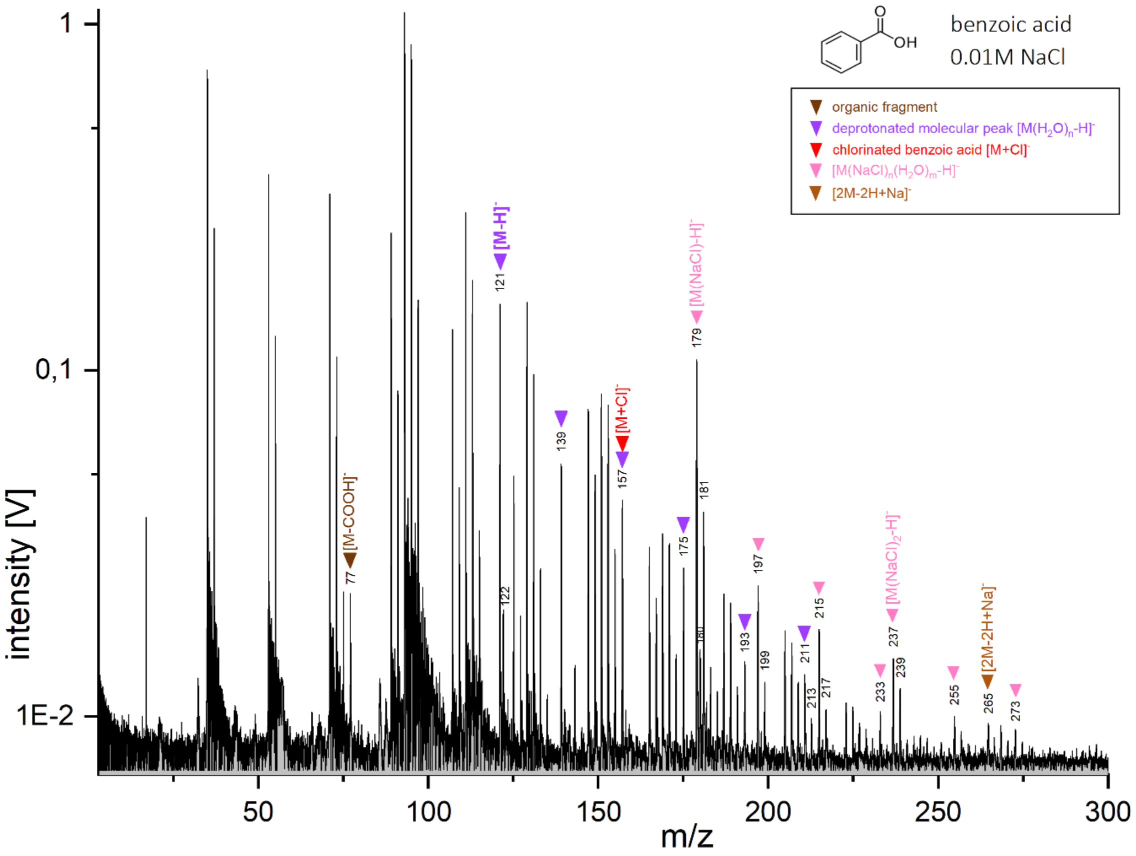

Figure S15. Baseline corrected anion mass spectrum of benzoic acid at a concentration of 0.17wt% in a H_2O and NaCl (0.01M) matrix, recorded at a delay time of 6.1µs.

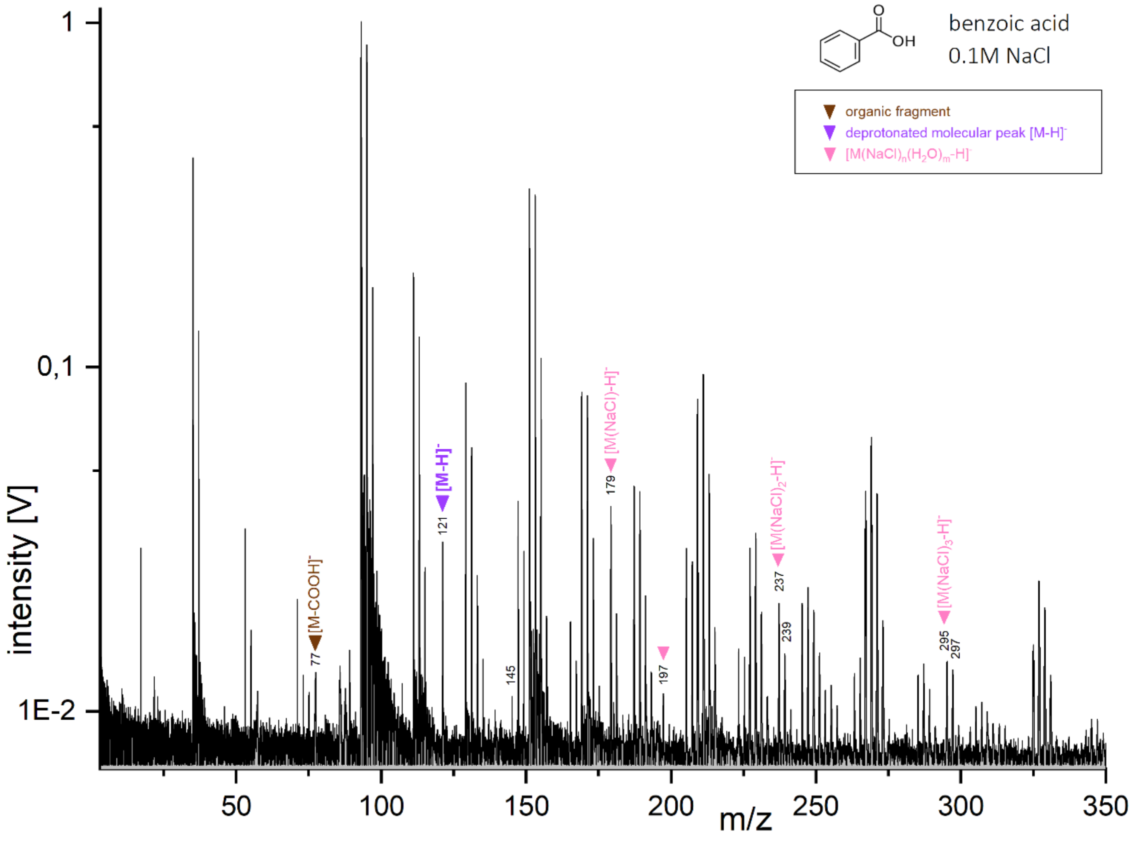

Figure S16. Baseline corrected anion mass spectrum of benzoic acid at a concentration of 0.17wt% in a H_2O and NaCl (0.1M) matrix, recorded at a delay time of 6.1µs.

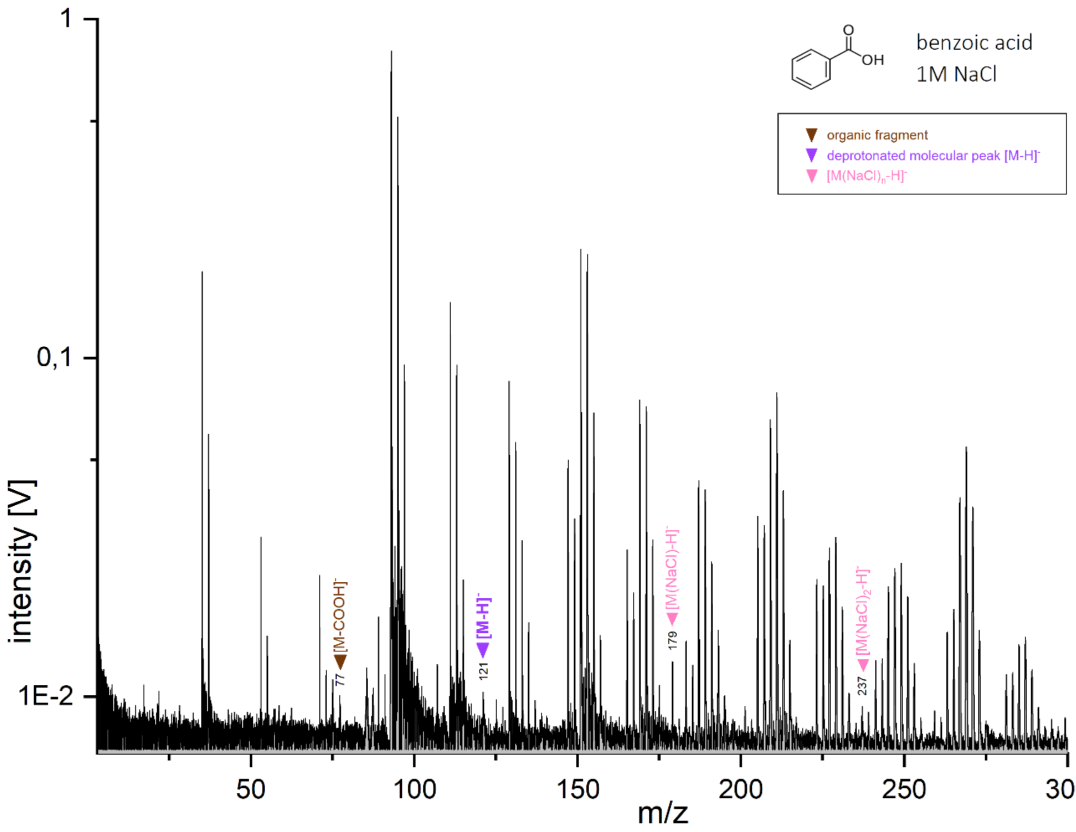

Figure S17. Baseline corrected anion mass spectrum of benzoic acid at a concentration of 0.14wt% in a H_2O and NaCl (1M) matrix, recorded at a delay time of 6.8µs.

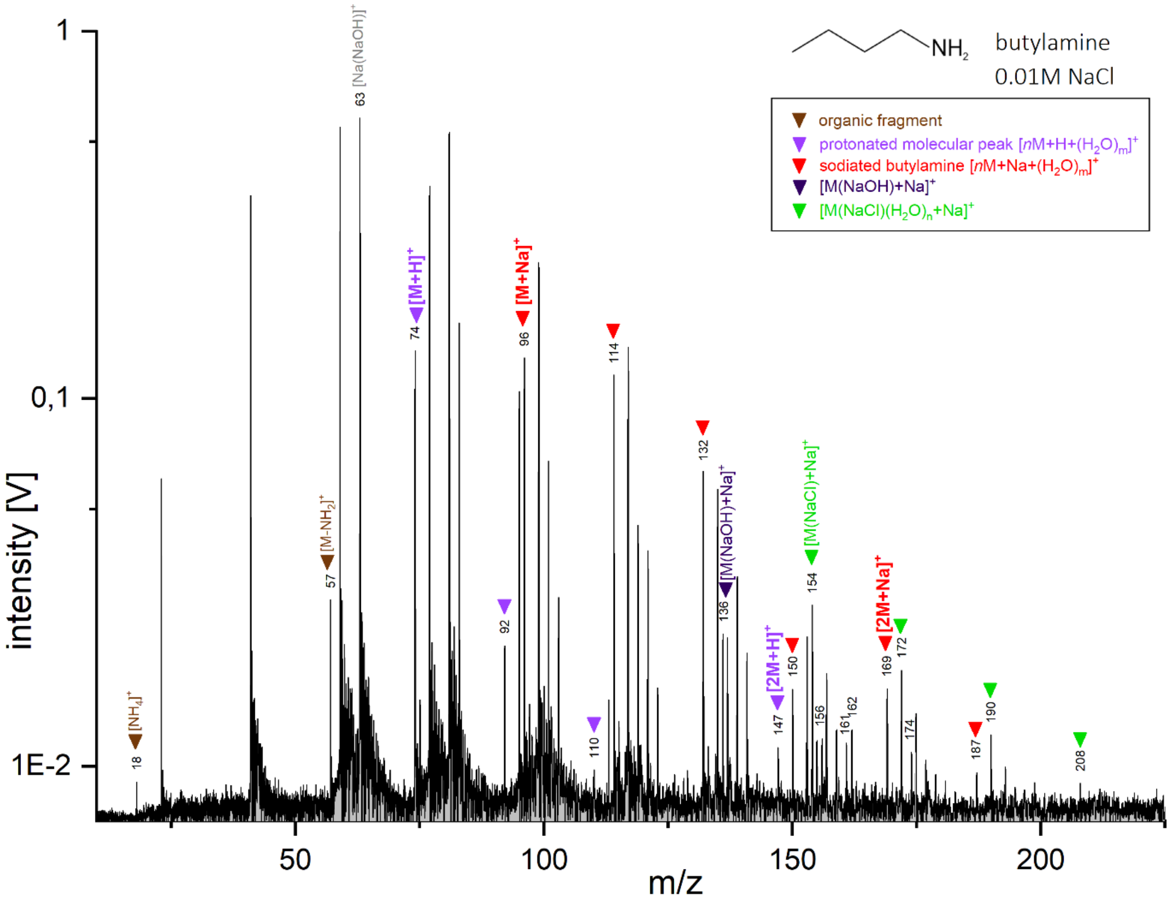

Figure S18. Baseline corrected cation mass spectrum of butylamine at a concentration of 5wt% in a H_2O and NaCl (0.01M) matrix, recorded at a delay time of 6.0µs.

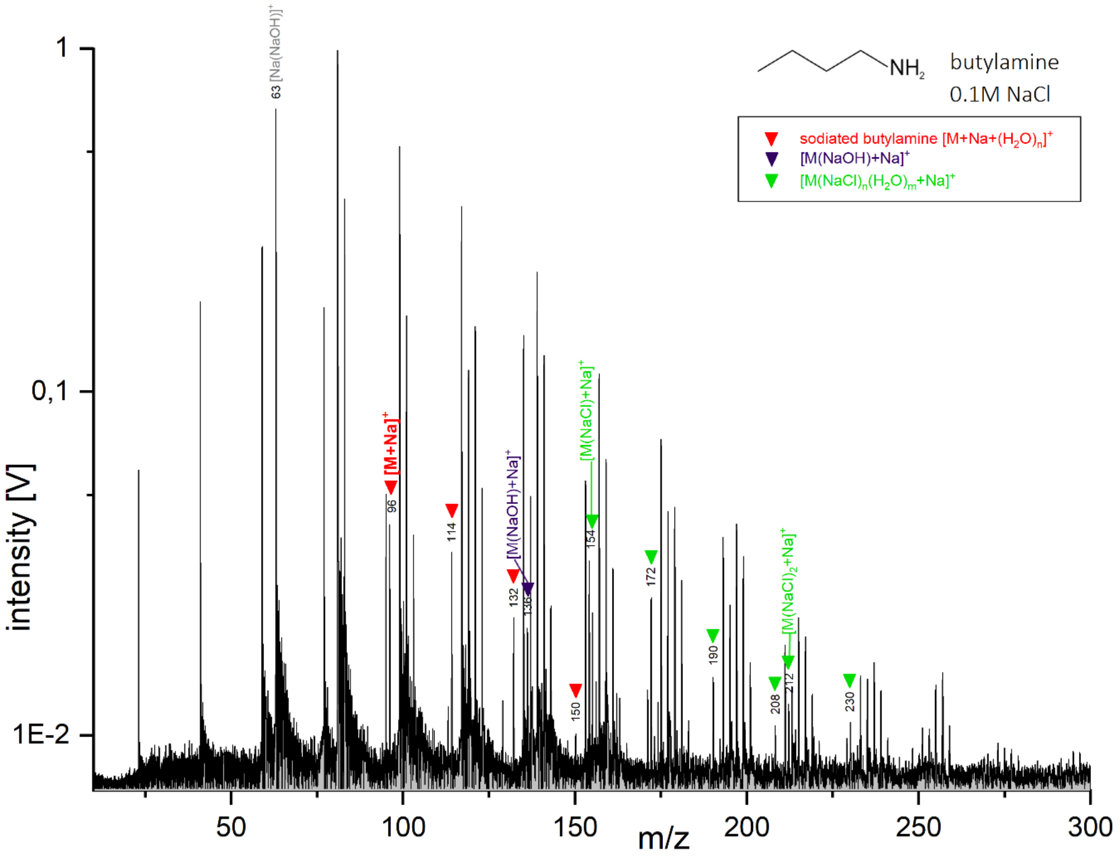

Figure S19. Baseline corrected cation mass spectrum of butylamine at a concentration of 5wt% in a H_2O and NaCl (0.1M) matrix, recorded at a delay time of 6.0µs. The peak at m/z 63 might have a contribution by organic species as it has a much higher amplitude than in the NaCl (0.1M) matrix spectra (Figure 2).

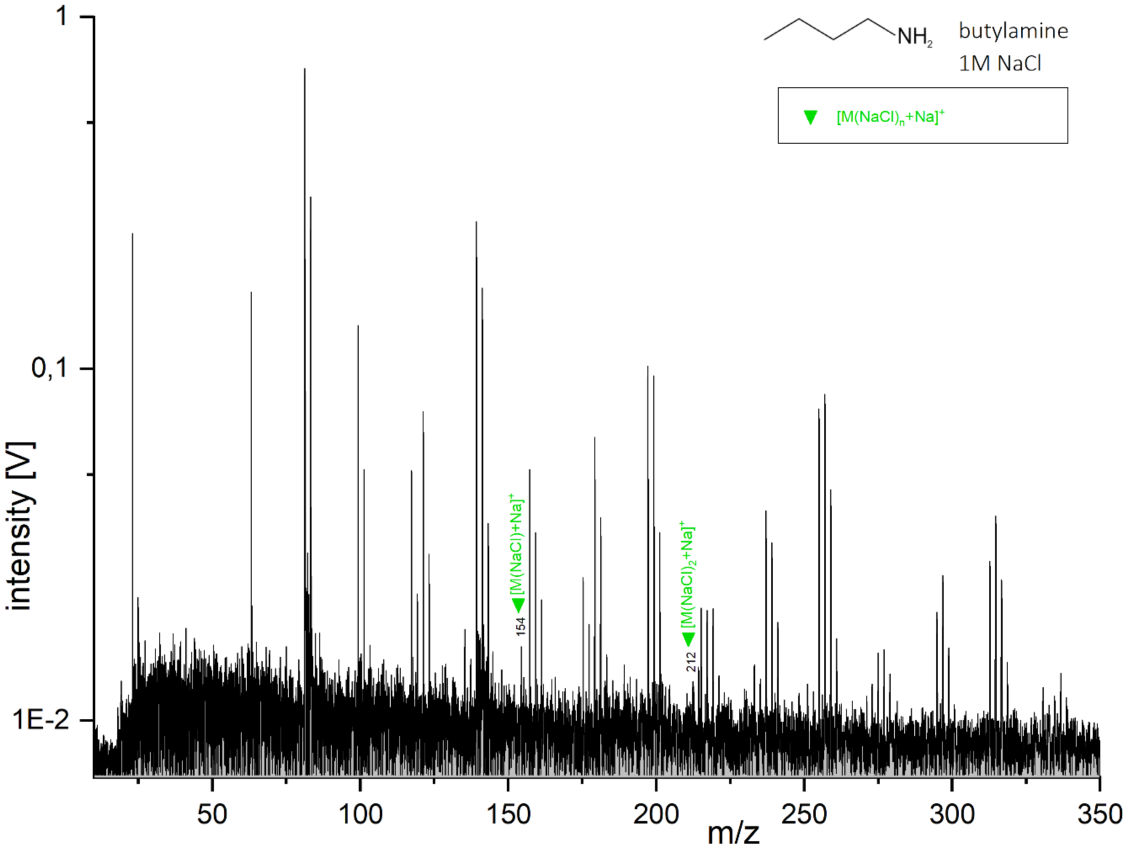

Figure S20. Baseline corrected cation mass spectrum of butylamine at a concentration of 5wt% in a H_2O and NaCl (1M) matrix, recorded at a delay time of 6.0µs.

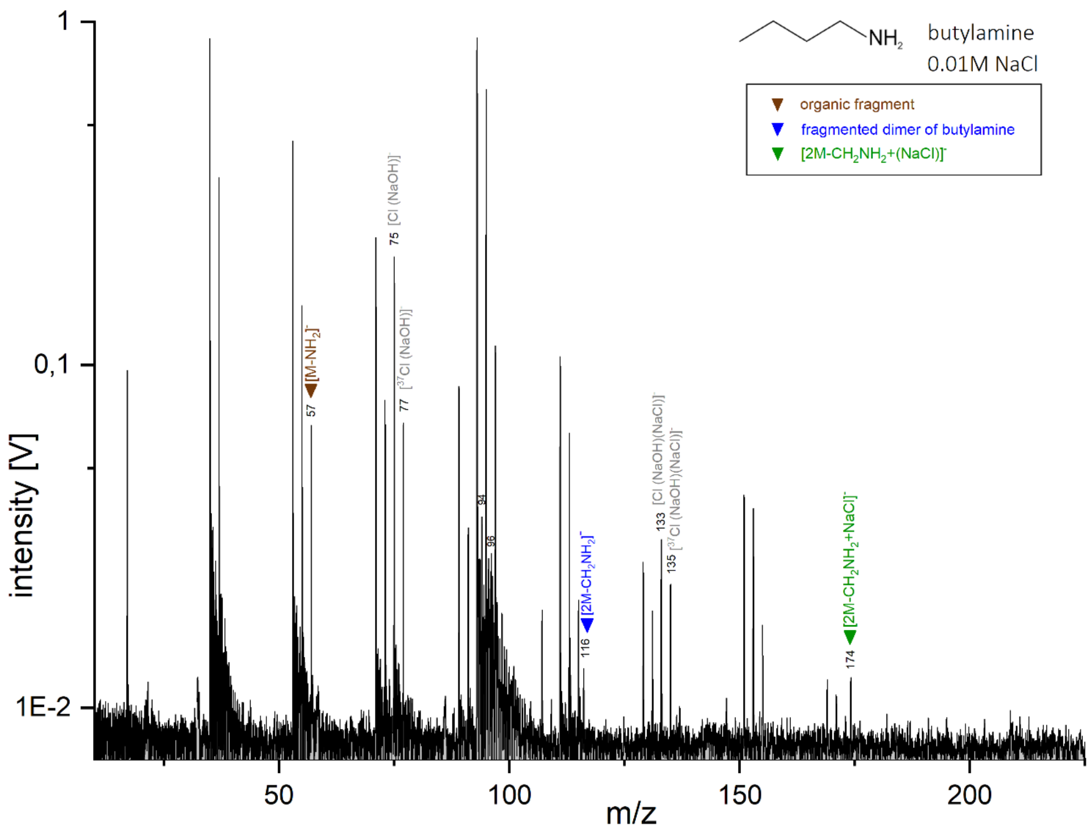

Figure S21. Baseline corrected anion mass spectrum of butylamine at a concentration of 5wt% in a H_2O and NaCl (0.01M) matrix, recorded at a delay time of 6.0µs. Peaks at m/z 75, 77, 133 and 135 may have a contribution by organic species as they have much higher amplitudes than in the NaCl (0.01M) matrix spectra (Figure S3).

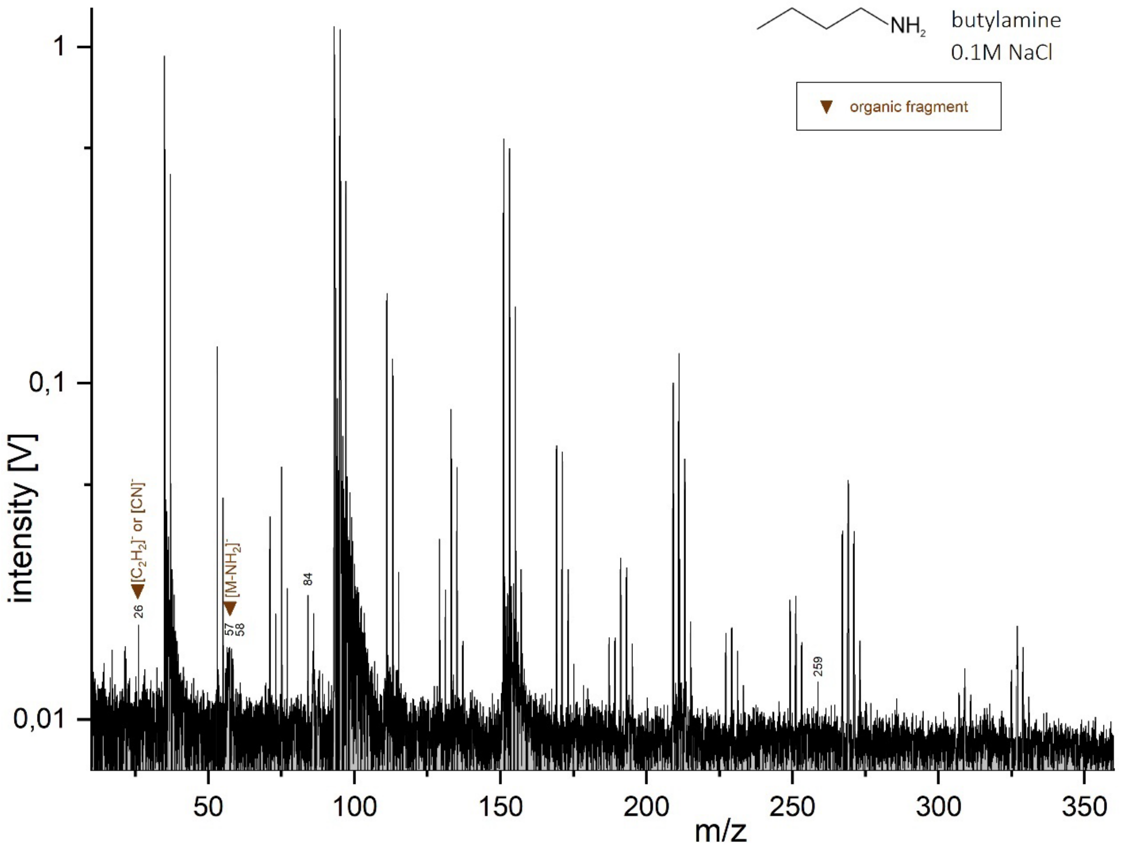

Figure S22. Baseline corrected anion mass spectrum of butylamine at a concentration of 5wt% in a H_2O and NaCl (0.1M) matrix, recorded at a delay time of 6.0µs.

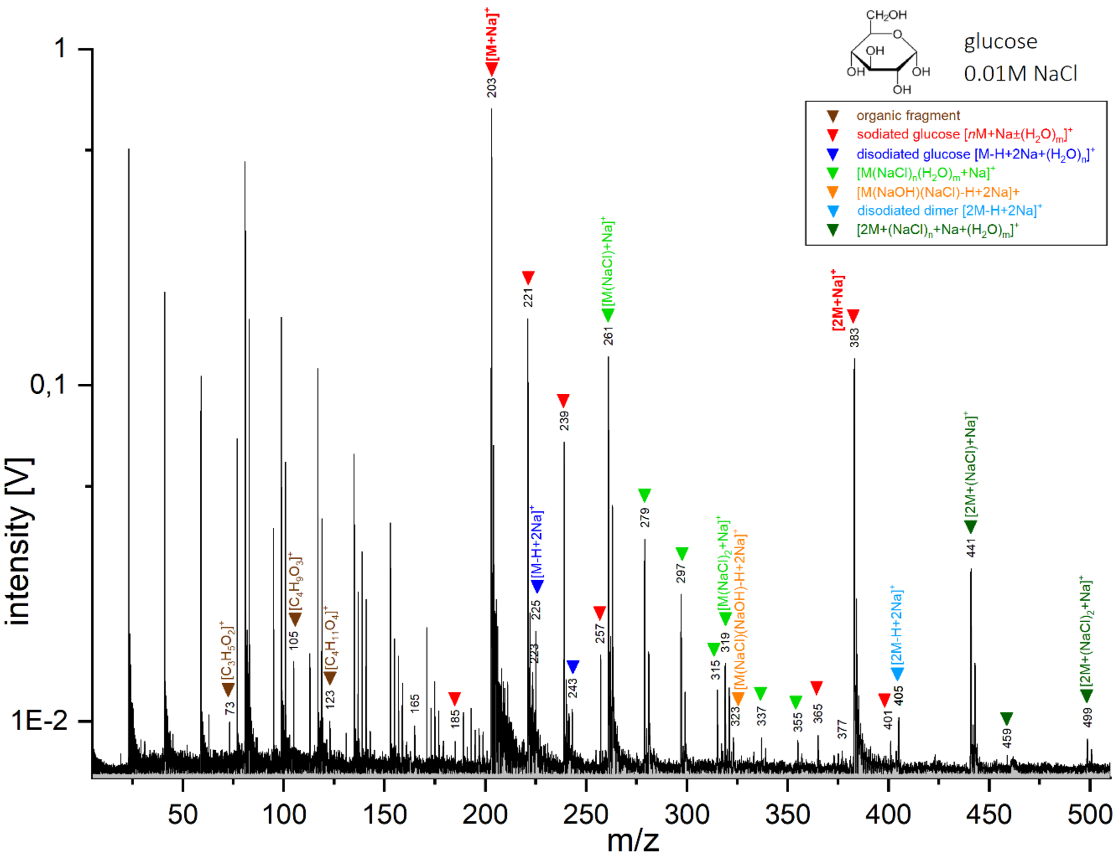

Figure S23. Baseline corrected cation mass spectrum of glucose at a concentration of 5wt% in a H_2O and NaCl (0.01M) matrix, recorded at a delay time of 6.2µs.

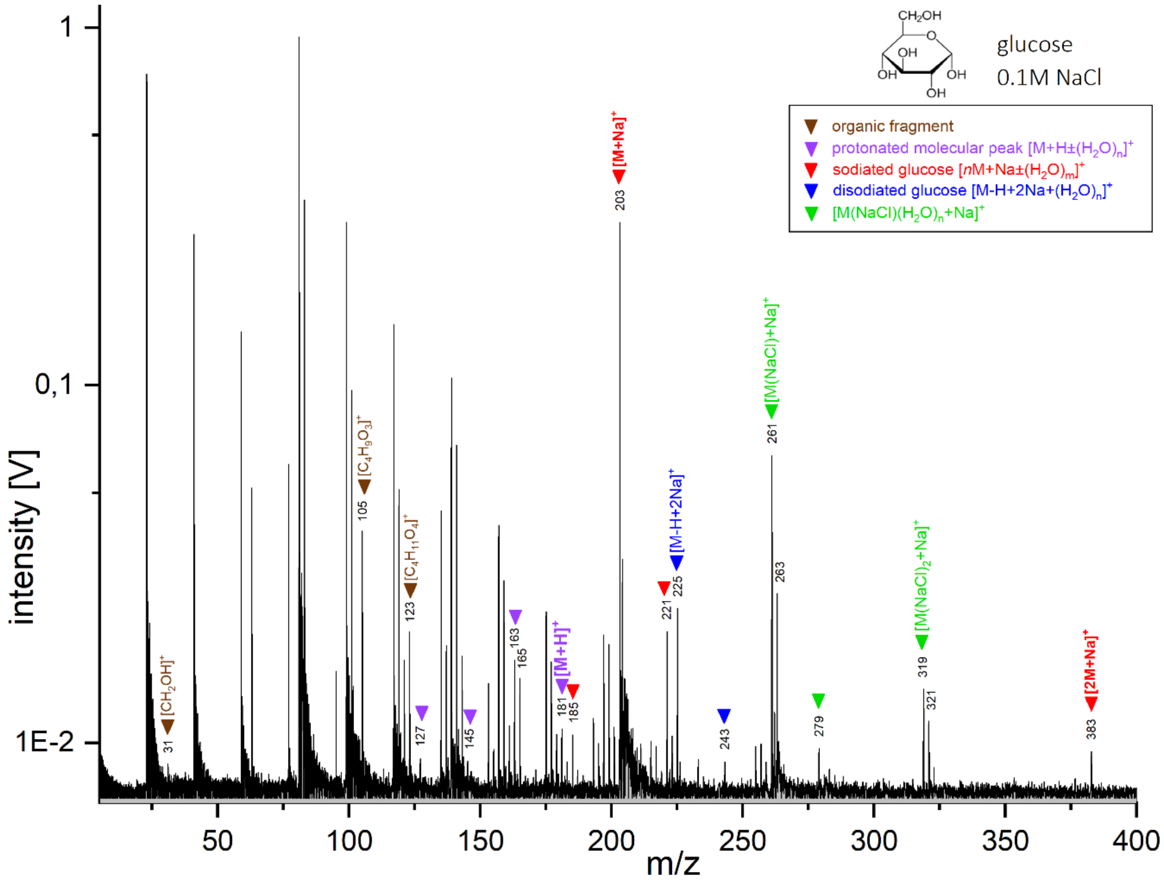

Figure S24. Baseline corrected cation mass spectrum of glucose at a concentration of 5wt% in a H_2O and NaCl (0.1M) matrix, recorded at a delay time of 5.7µs.

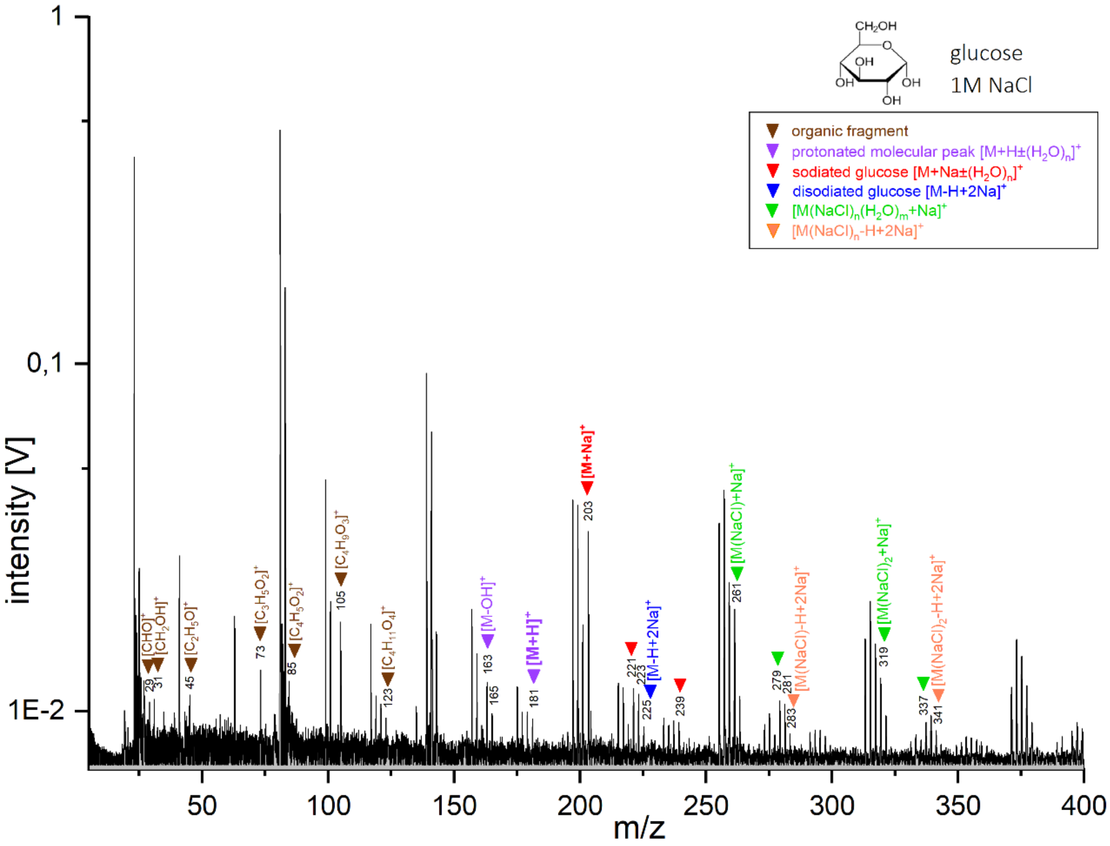

Figure S25. Baseline corrected cation mass spectrum of glucose at a concentration of 5wt% in a H_2O and NaCl (1M) matrix, recorded at a delay time of 6.2µs. The peak at m/z 181u (0.0095 V) is assigned to both the salt cluster $[Na(NaOH)(NaCl)_2]^+$ (0.0064 V) and protonated glucose $[M+H]^+$ (0.0031 V).

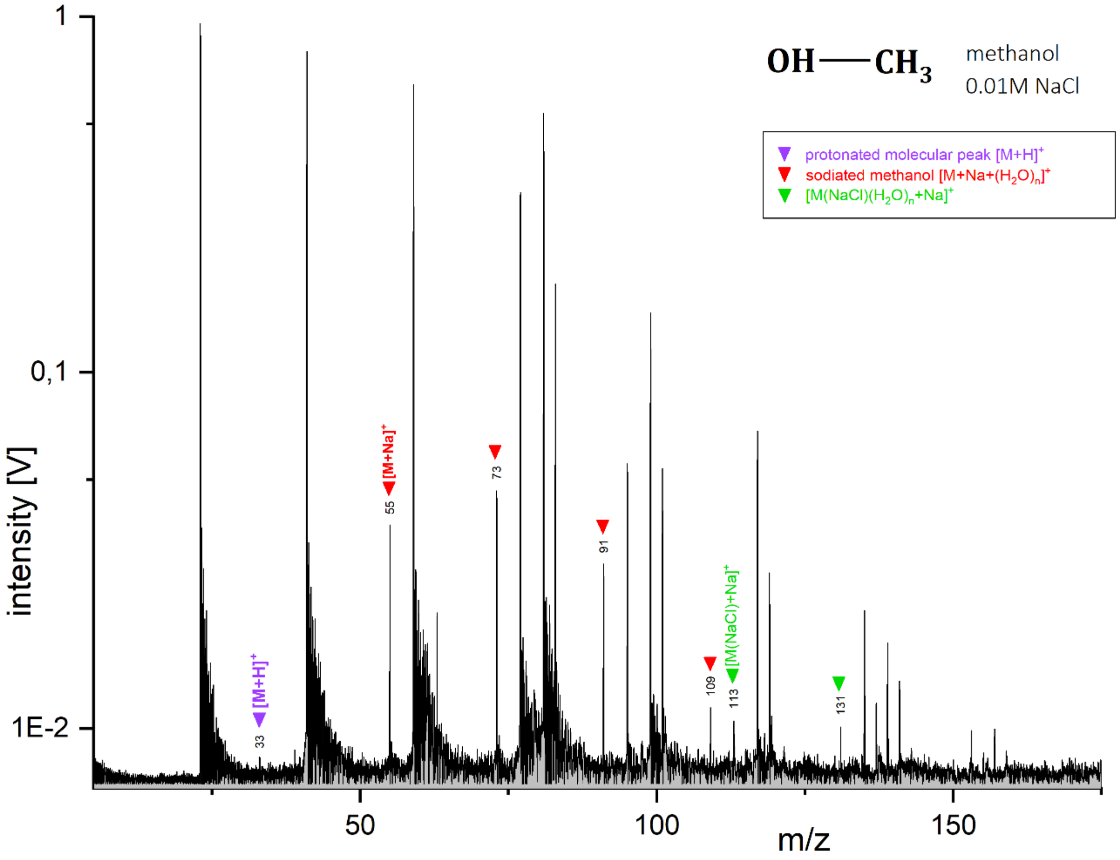

Figure S26. Baseline corrected cation mass spectrum of methanol at a concentration of 5wt% in a H_2O and NaCl (0.01M) matrix, recorded at a delay time of 5.5µs.

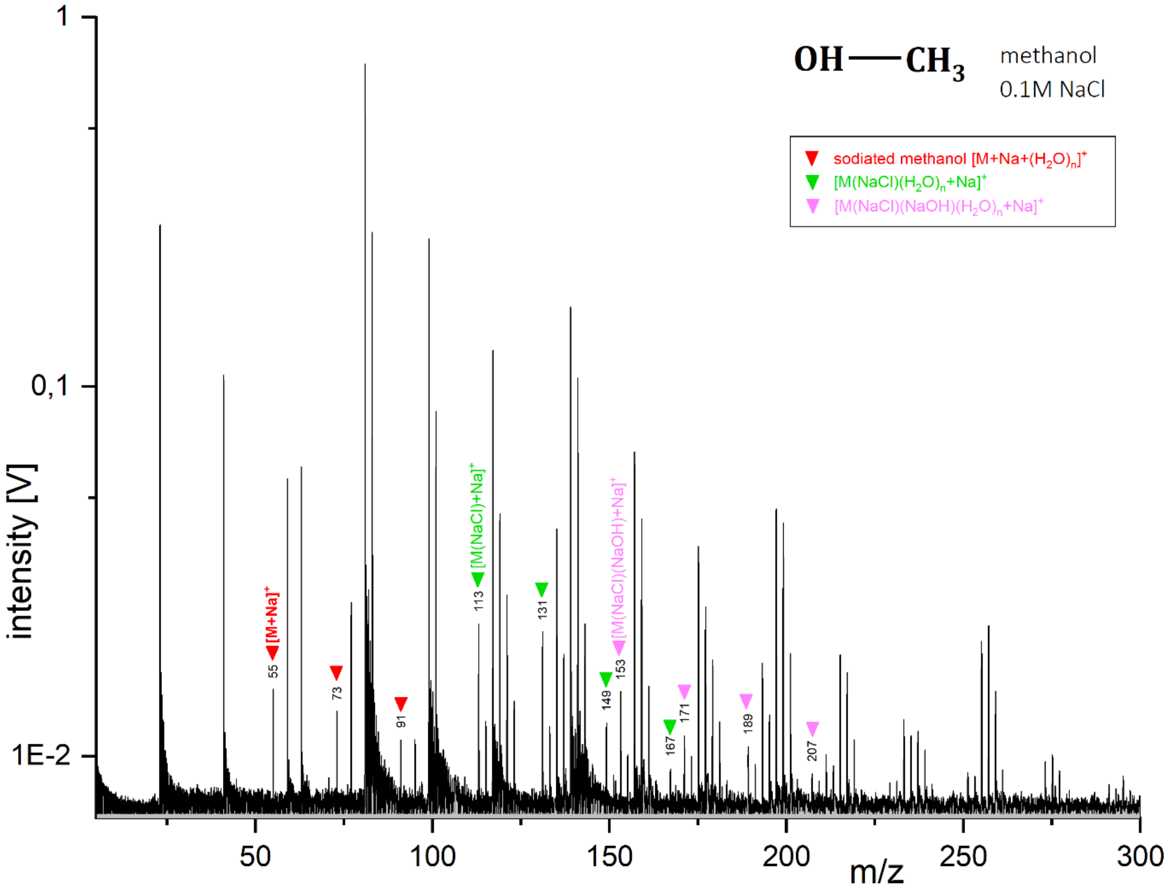

Figure S27. Baseline corrected cation mass spectrum of methanol at a concentration of 5wt% in a H_2O and NaCl (0.1M) matrix, recorded at a delay time of 5.9µs.

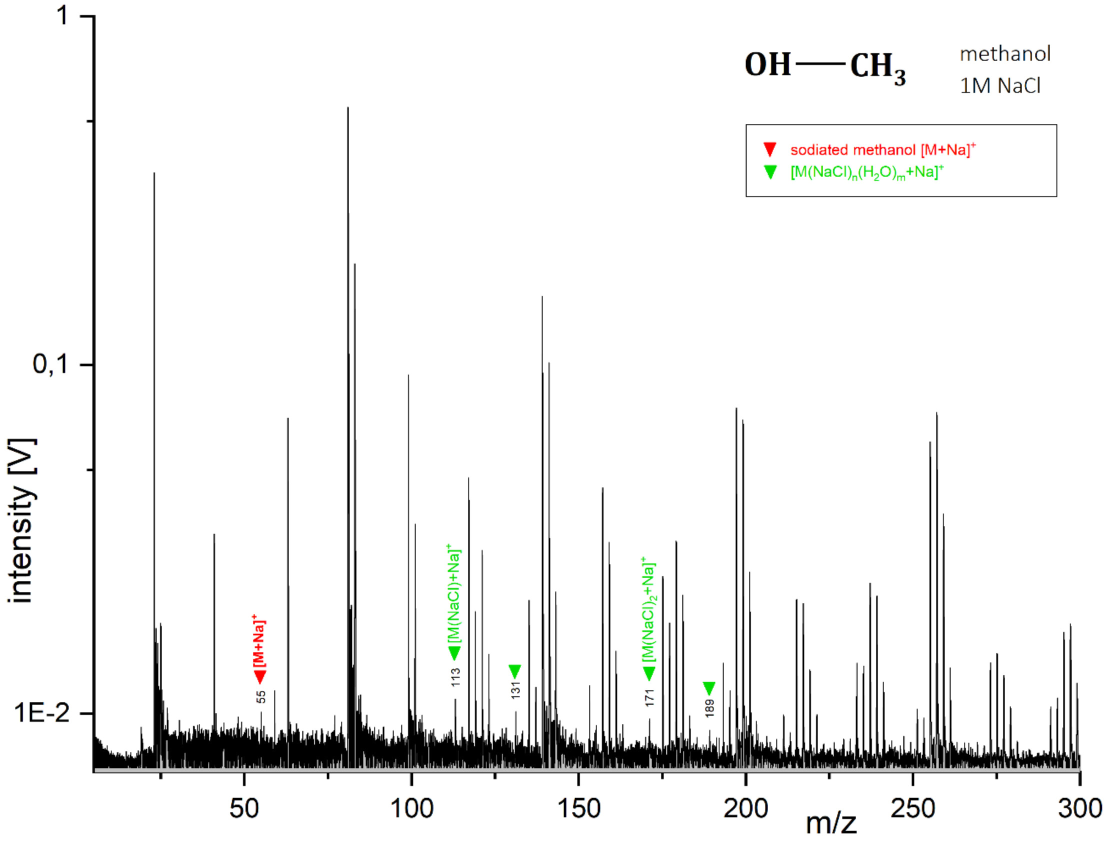

Figure S28. Baseline corrected cation mass spectrum of methanol at a concentration of 5wt% in a H_2O and NaCl (1M) matrix, recorded at a delay time of 6.2µs.

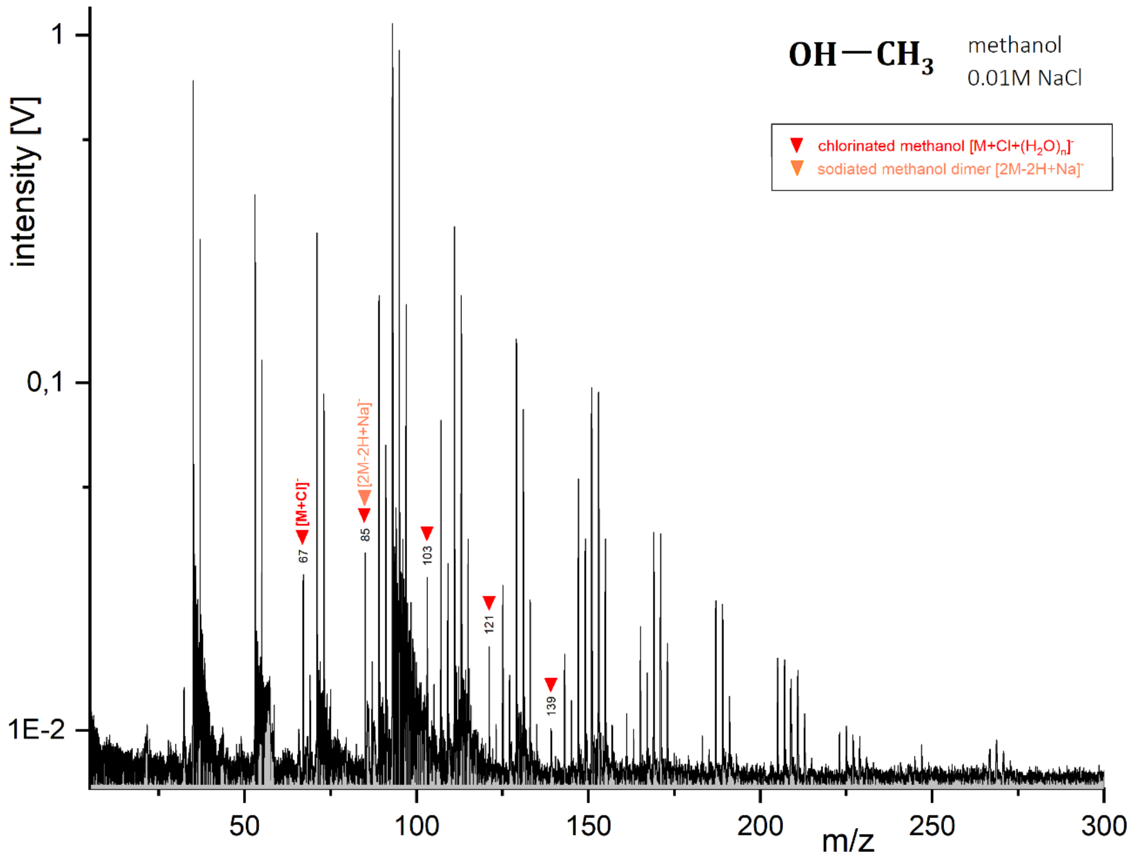

Figure S29. Baseline corrected anion mass spectrum of methanol at a concentration of 5wt% in a H_2O and NaCl (0.01M) matrix, recorded at a delay time of 6.1µs.

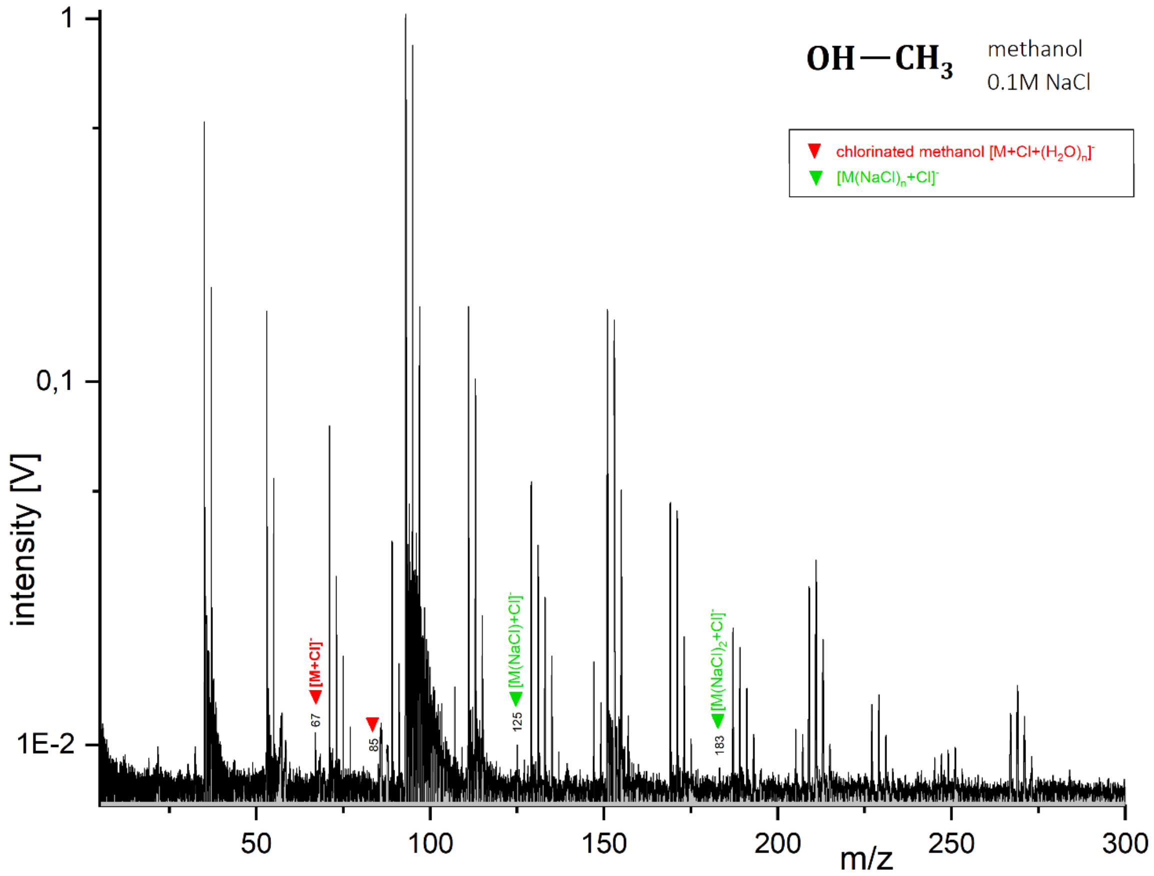

Figure S30. Baseline corrected anion mass spectrum of methanol at a concentration of 5wt% in a H_2O and NaCl (0.1M) matrix, recorded at a delay time of 6.0µs.

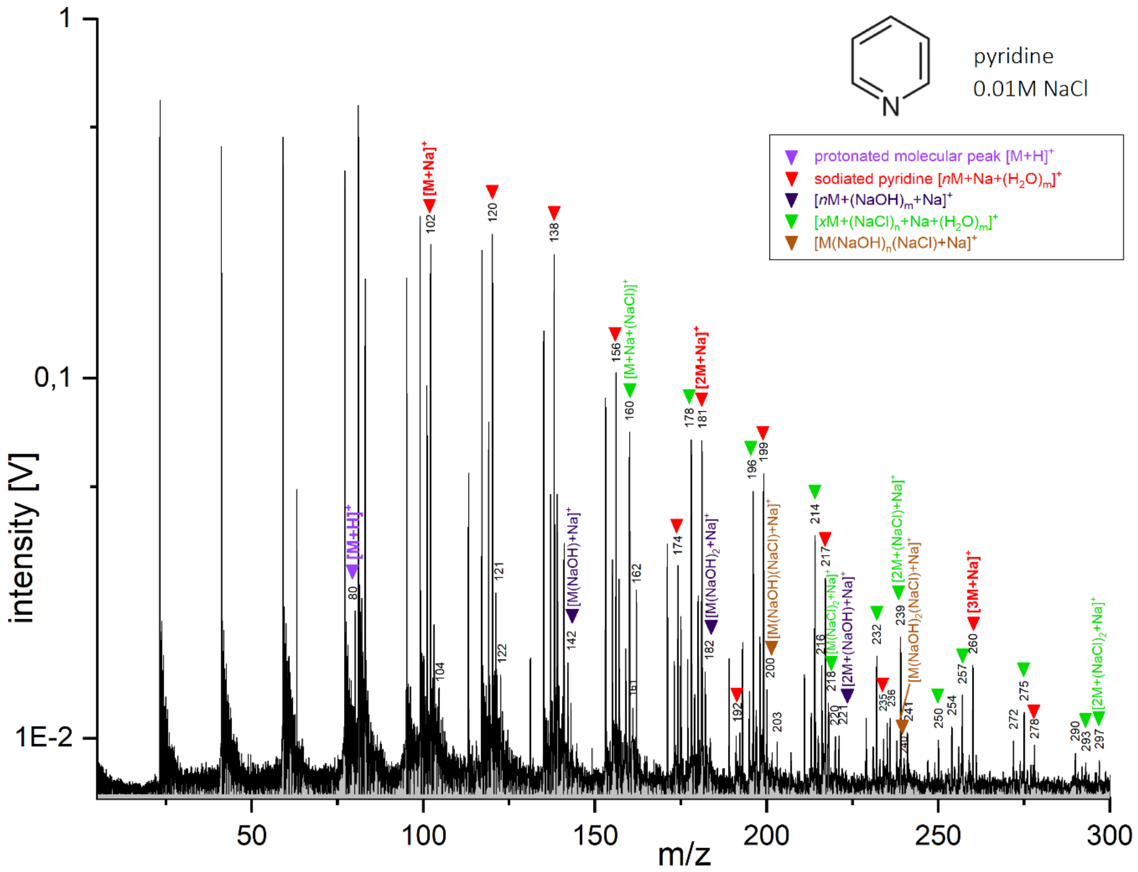

Figure S31. Baseline corrected cation mass spectrum of pyridine at a concentration of 5wt% in a H_2O and NaCl (0.01M) matrix, recorded at a delay time of 6.2µs.

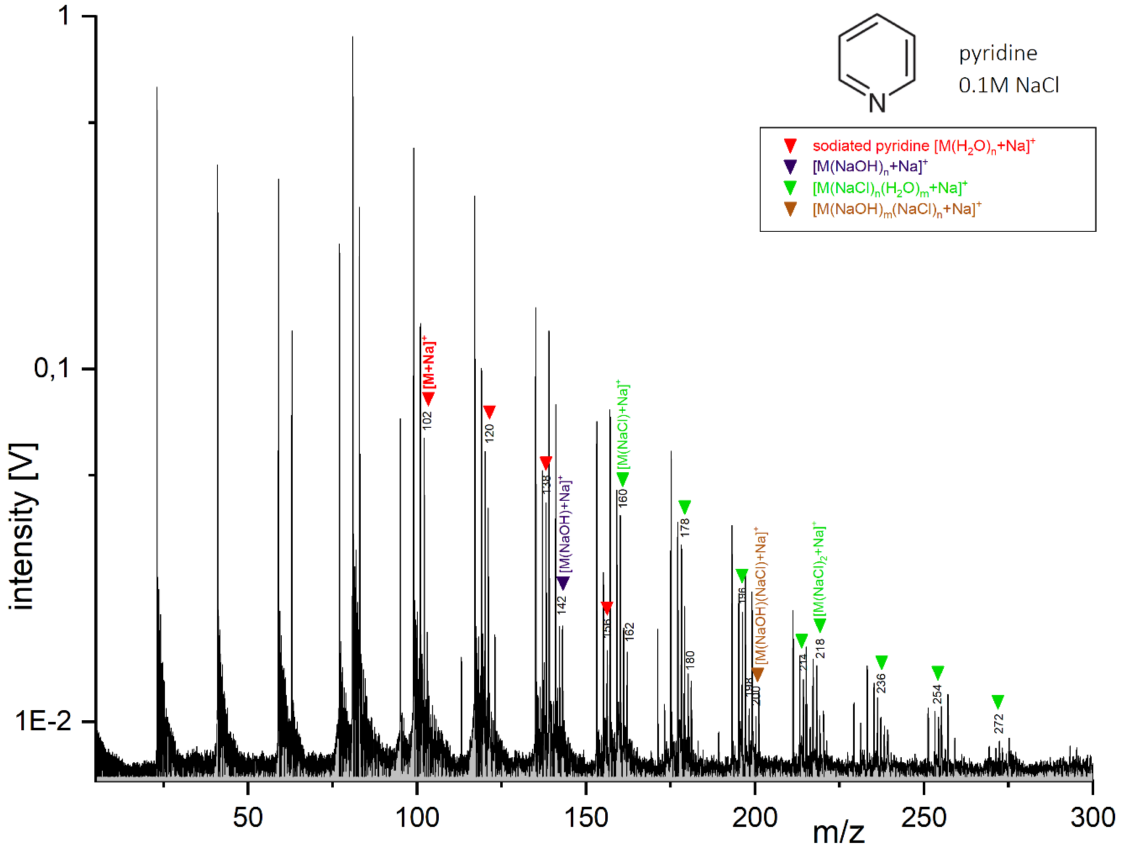

Figure S32. Baseline corrected cation mass spectrum of pyridine at a concentration of 5wt% in a H_2O and NaCl (0.1M) matrix, recorded at a delay time of 6.0µs.

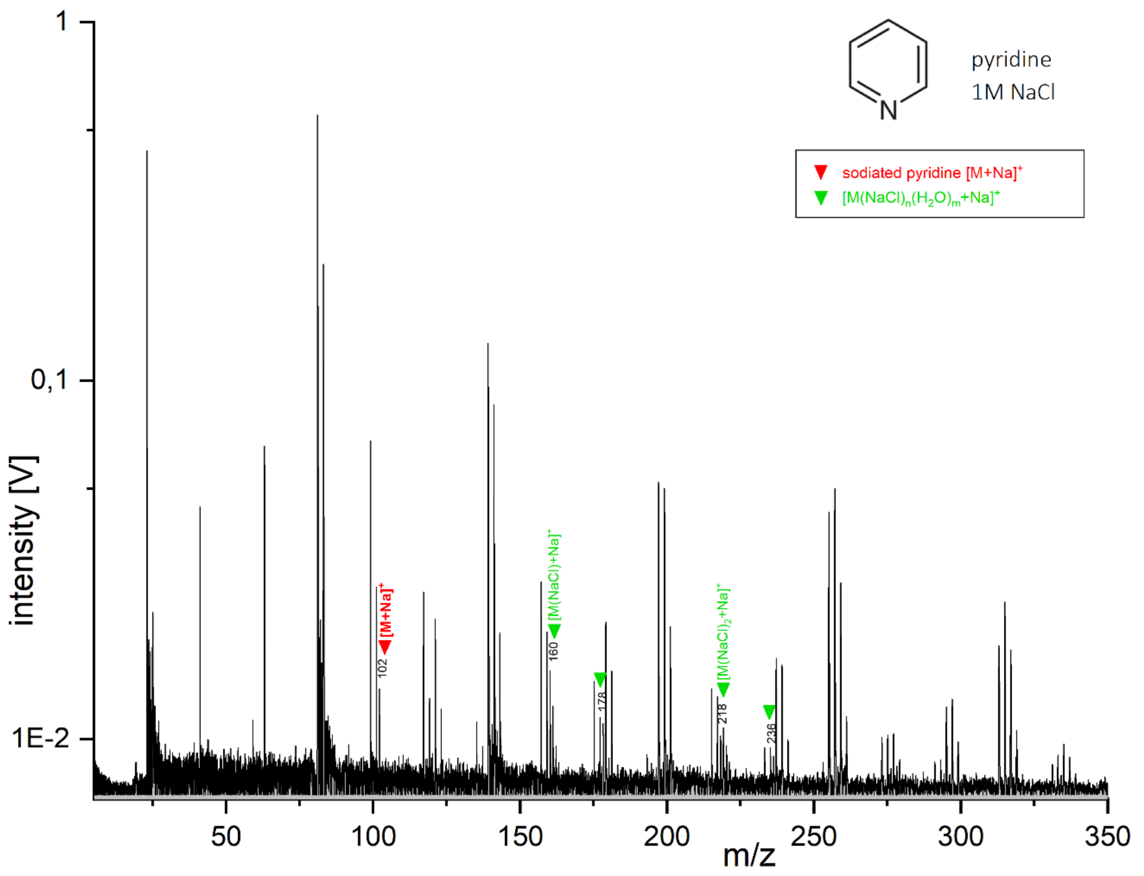

Figure S33. Baseline corrected cation mass spectrum of pyridine at a concentration of 5wt% in a H_2O and NaCl (1M) matrix, recorded at a delay time of 6.2µs.

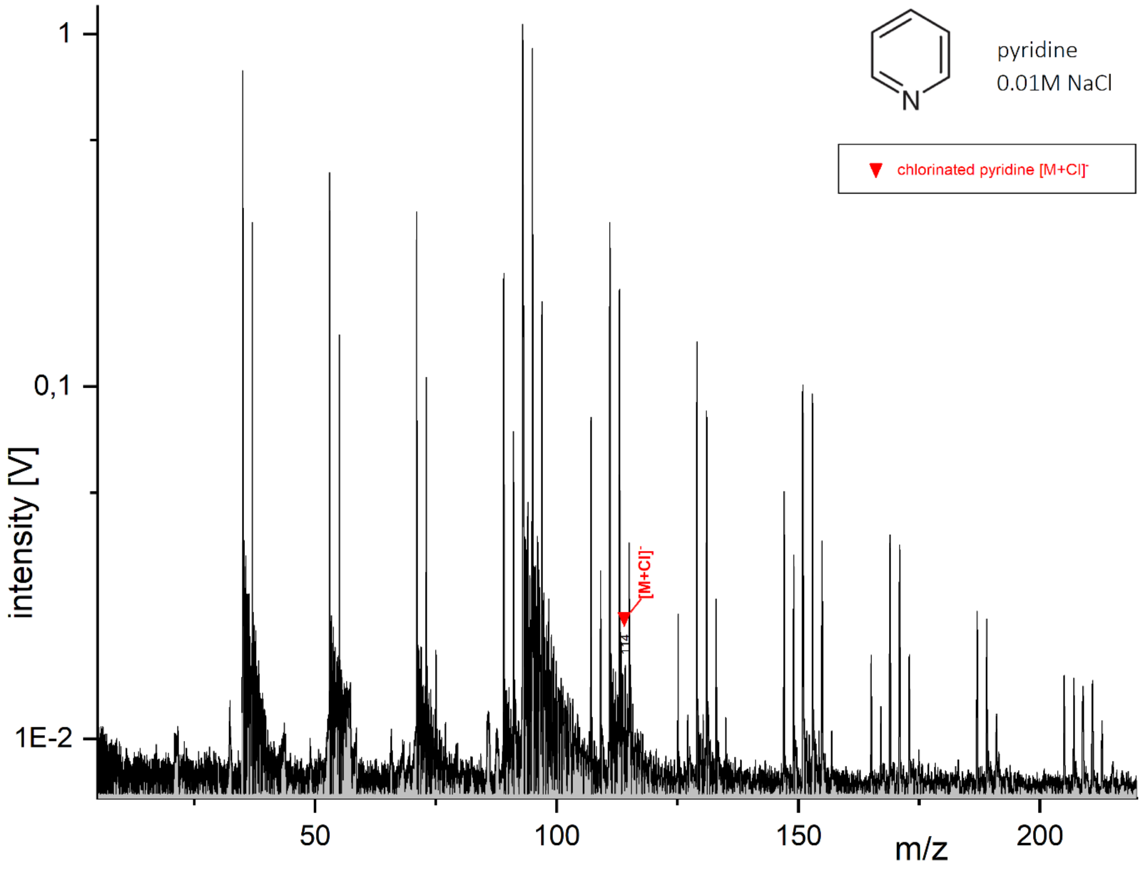

Figure S34. Baseline corrected anion mass spectrum of pyridine at a concentration of 5wt% in a H_2O and NaCl (0.01M) matrix, recorded at a delay time of 6.1µs.

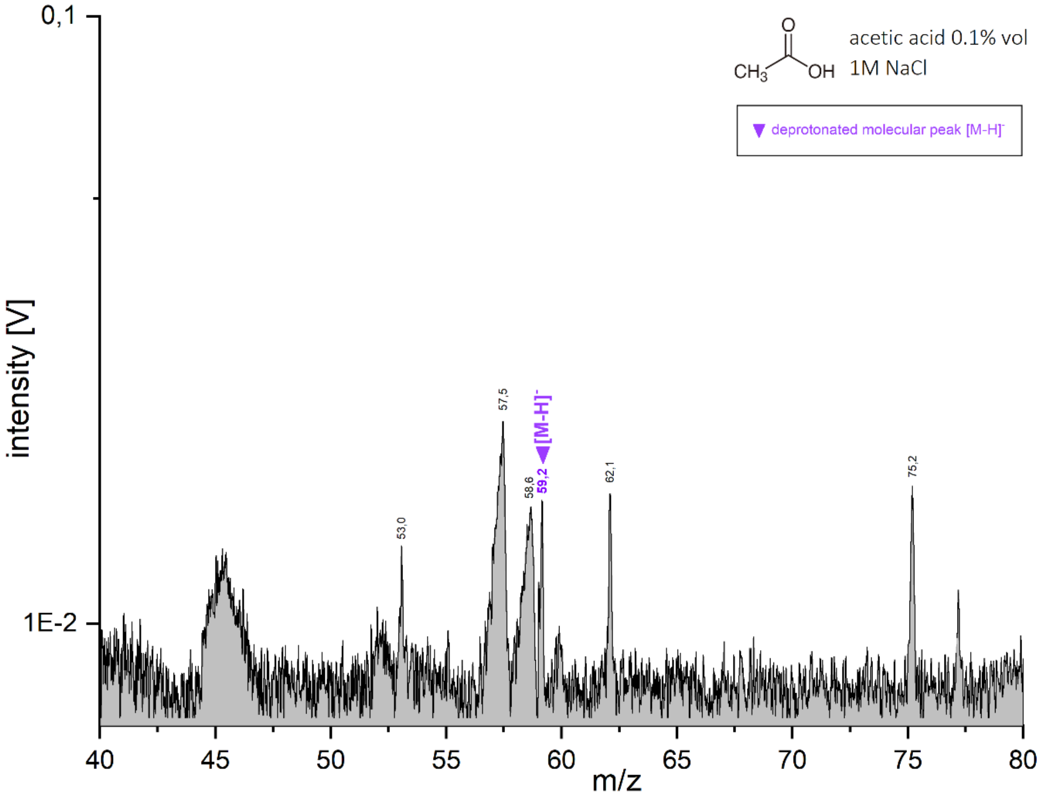

Figure S35. Section of a baseline corrected anion mass spectrum of acetic acid at a concentration of 0.1wt% in a H_2O and NaCl (1M) matrix, recorded at a delay time of 7.5µs. Peaks labelled in black originate exclusively from the salty matrix.

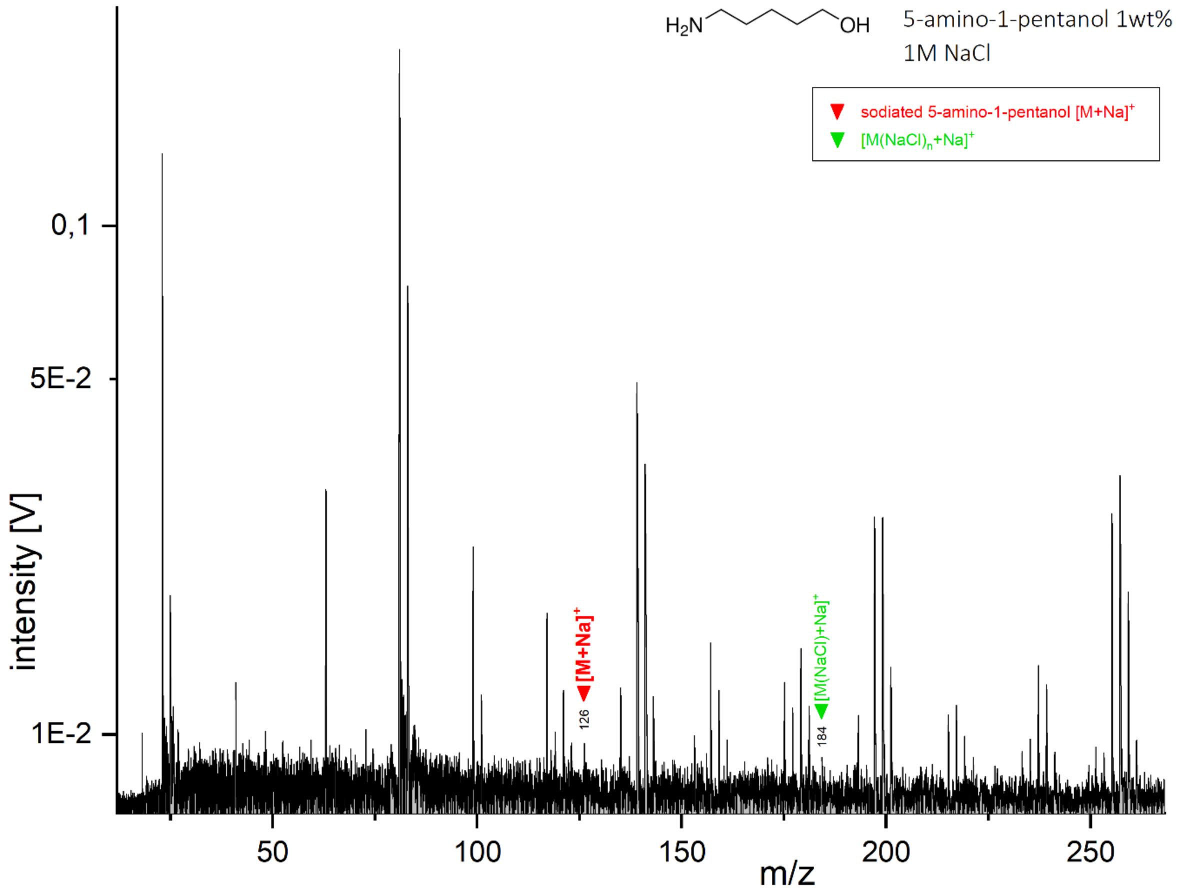

Figure S36. Baseline corrected cation mass spectrum of 5-amino-1-pentanol at a concentration of 1wt% in a H_2O and NaCl (1M) matrix, recorded at a delay time of 6.5µs.

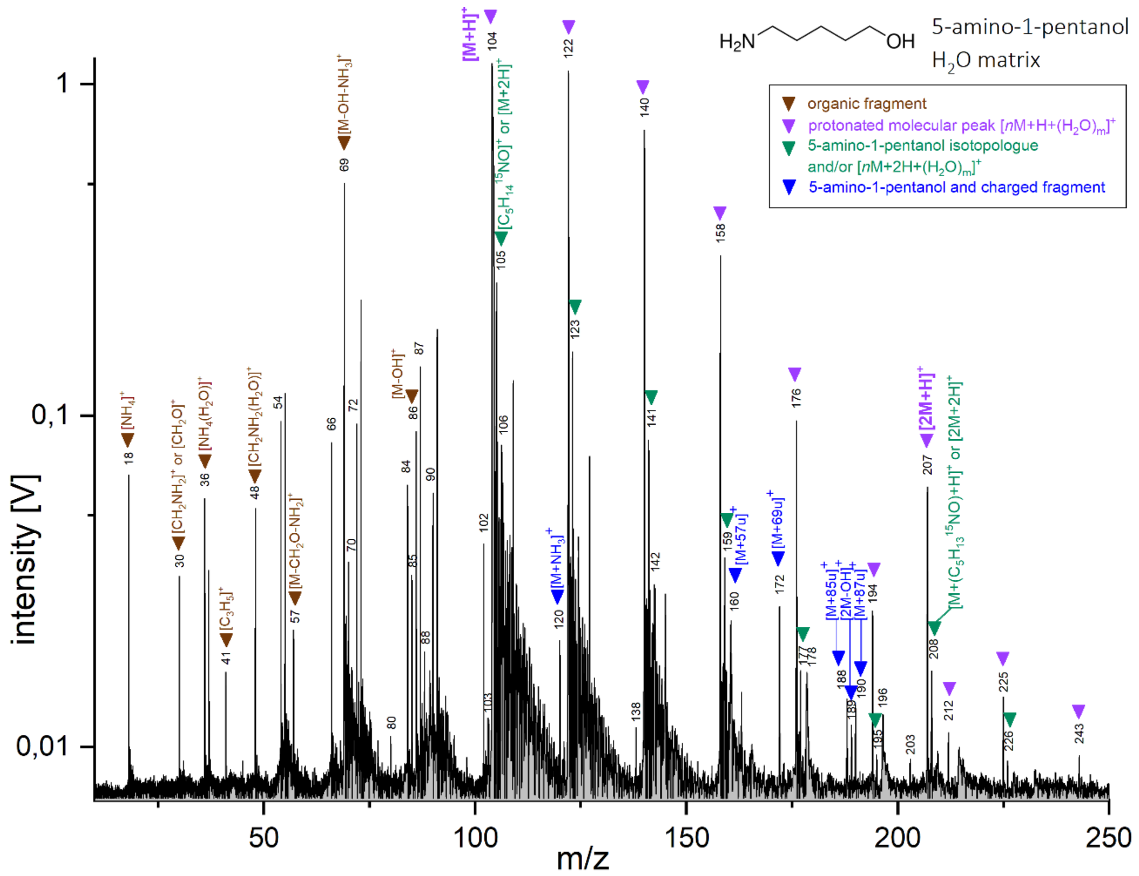

Figure S37. Baseline corrected cation mass spectrum of 5-amino-1-pentanol at a concentration of 5wt% in a pure H_2O matrix, recorded at a delay time of 6.3µs. Unlabeled peaks originate exclusively from the water matrix.

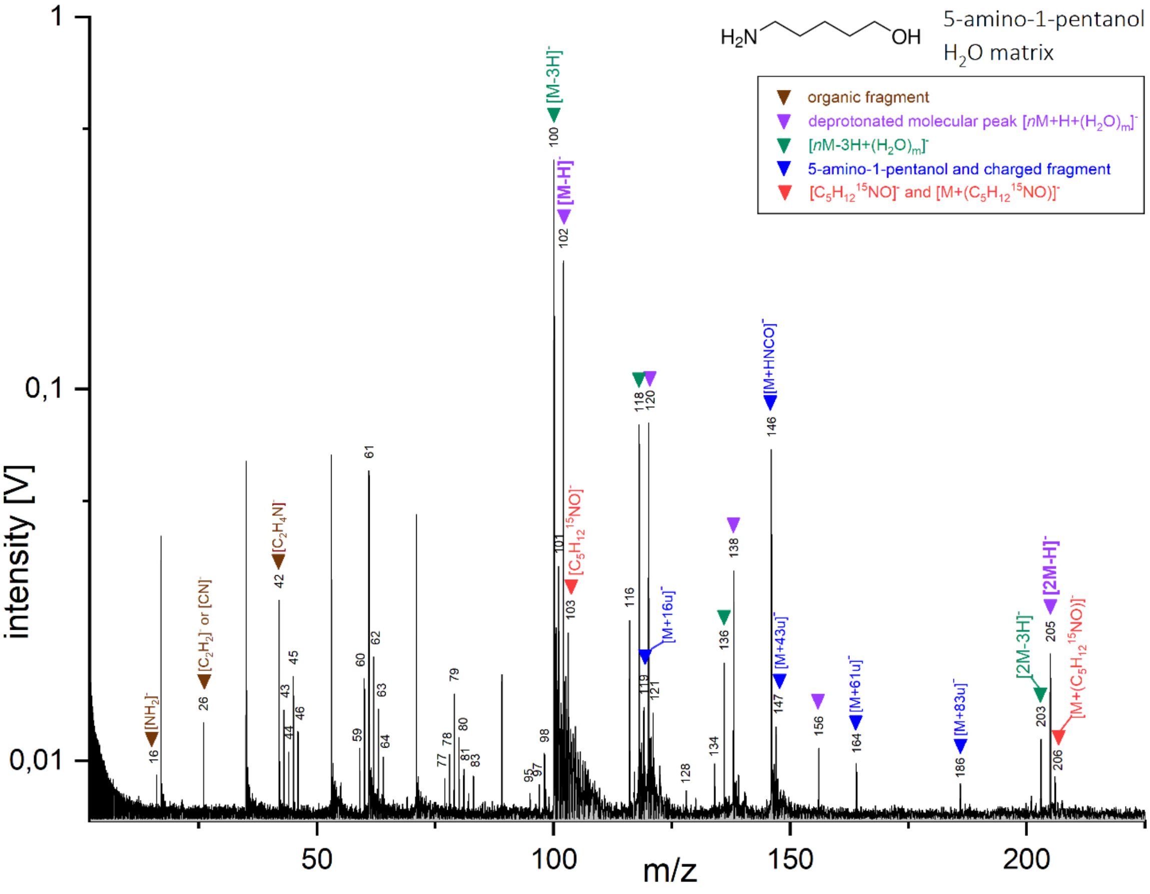

Figure S38. Baseline corrected anion mass spectrum of 5-amino-1-pentanol at a concentration of 5wt% in a pure H_2O matrix, recorded at a delay time of 5.7µs. Unlabeled peaks originate exclusively from the water matrix.

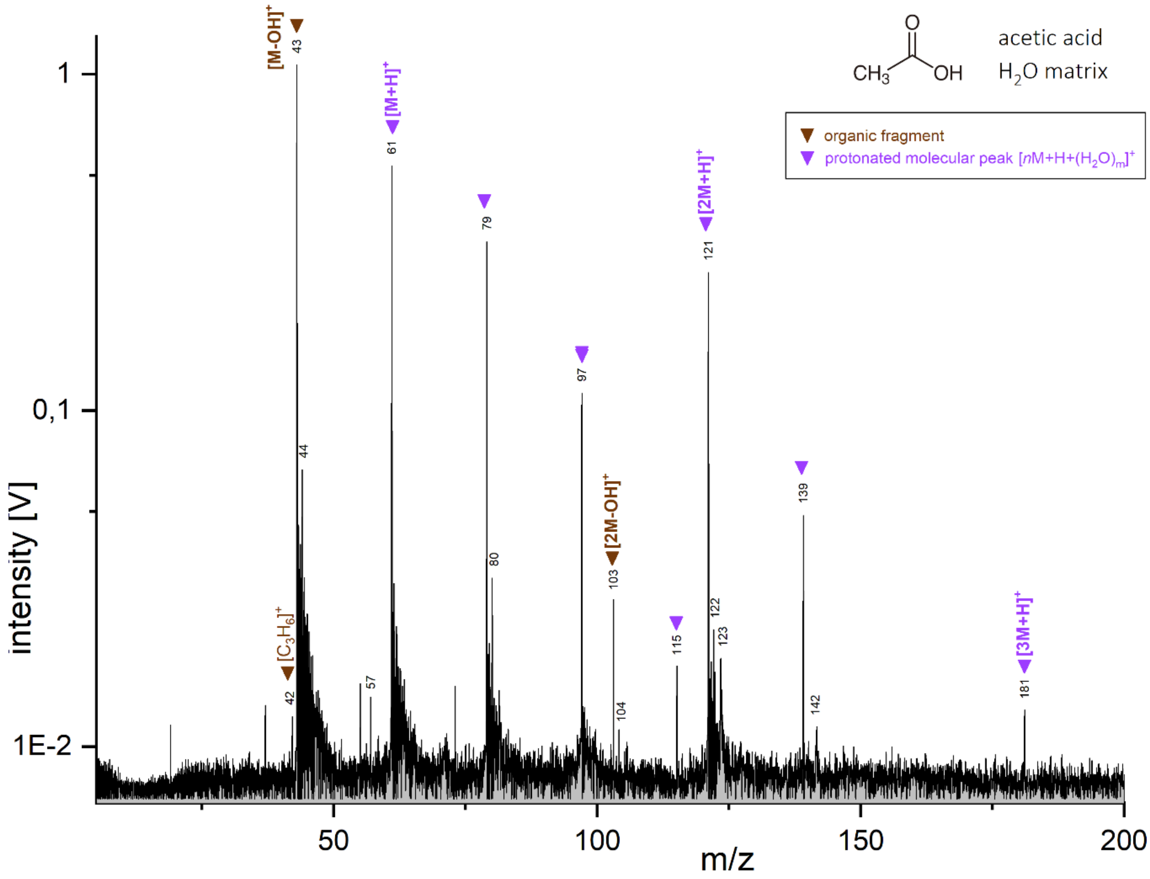

Figure S39. Baseline corrected cation mass spectrum of acetic acid at a concentration of 5wt% in a pure H_2O matrix, recorded at a delay time of 5.7µs. Unlabeled peaks originate exclusively from the water matrix.

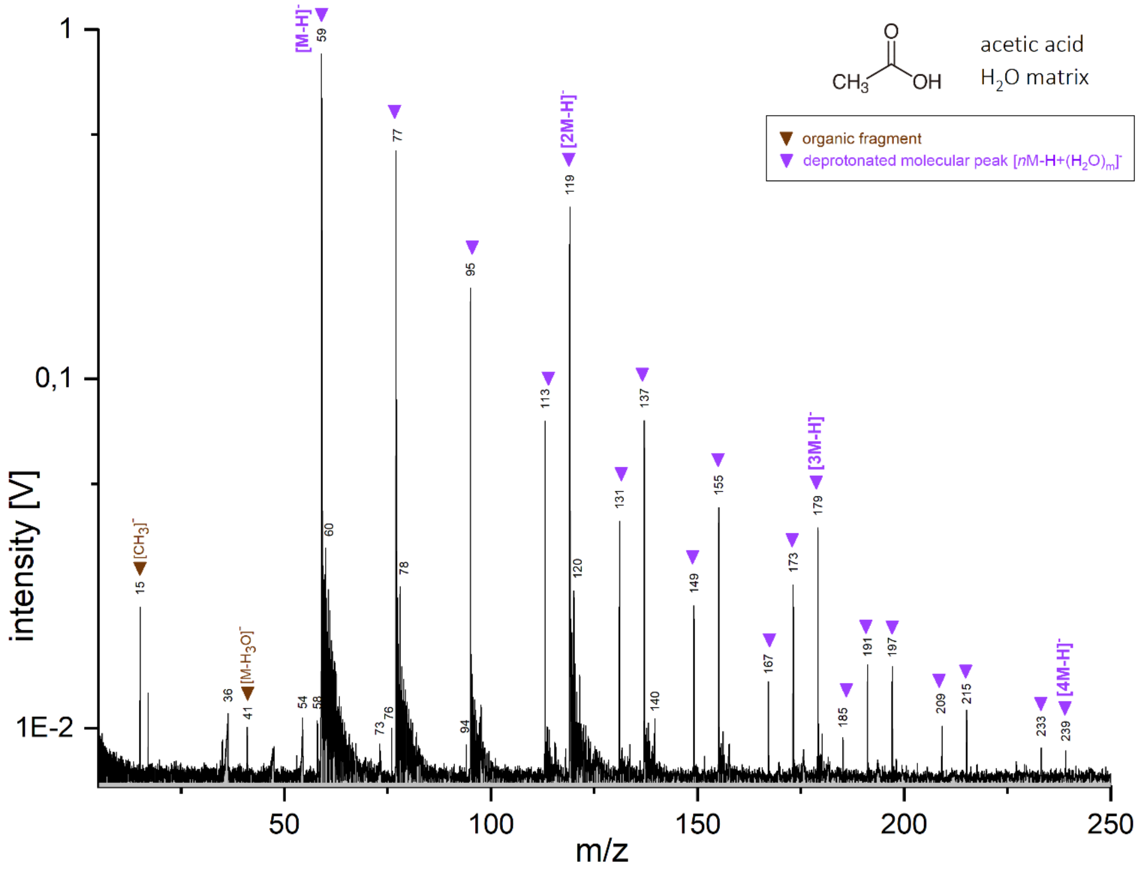

Figure S40. Baseline corrected anion mass spectrum of acetic acid at a concentration of 5wt% in a pure H_2O matrix, recorded at a delay time of 6.3µs. Unlabeled peaks originate exclusively from the water matrix.

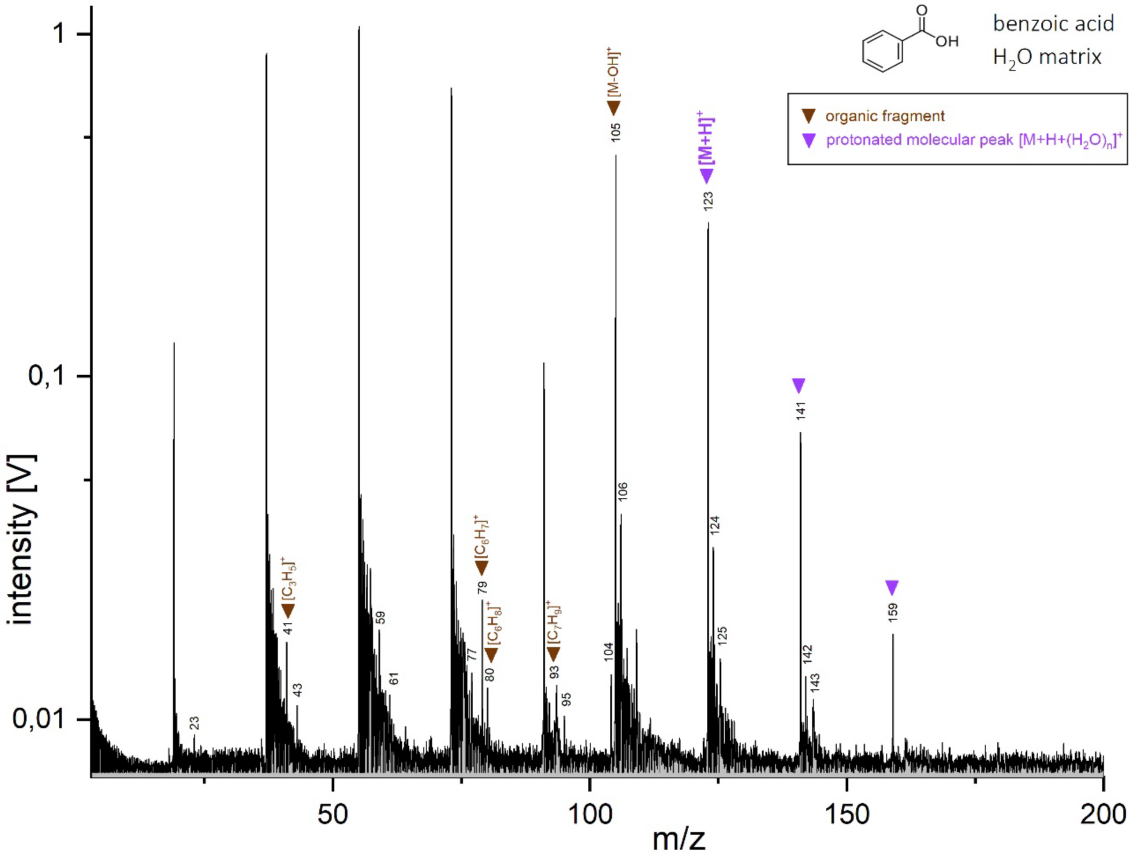

Figure S41. Baseline corrected cation mass spectrum of benzoic acid at a concentration of 0.17wt% in a pure H_2O matrix, recorded at a delay time of 5.7µs. Unlabeled peaks originate exclusively from the water matrix.

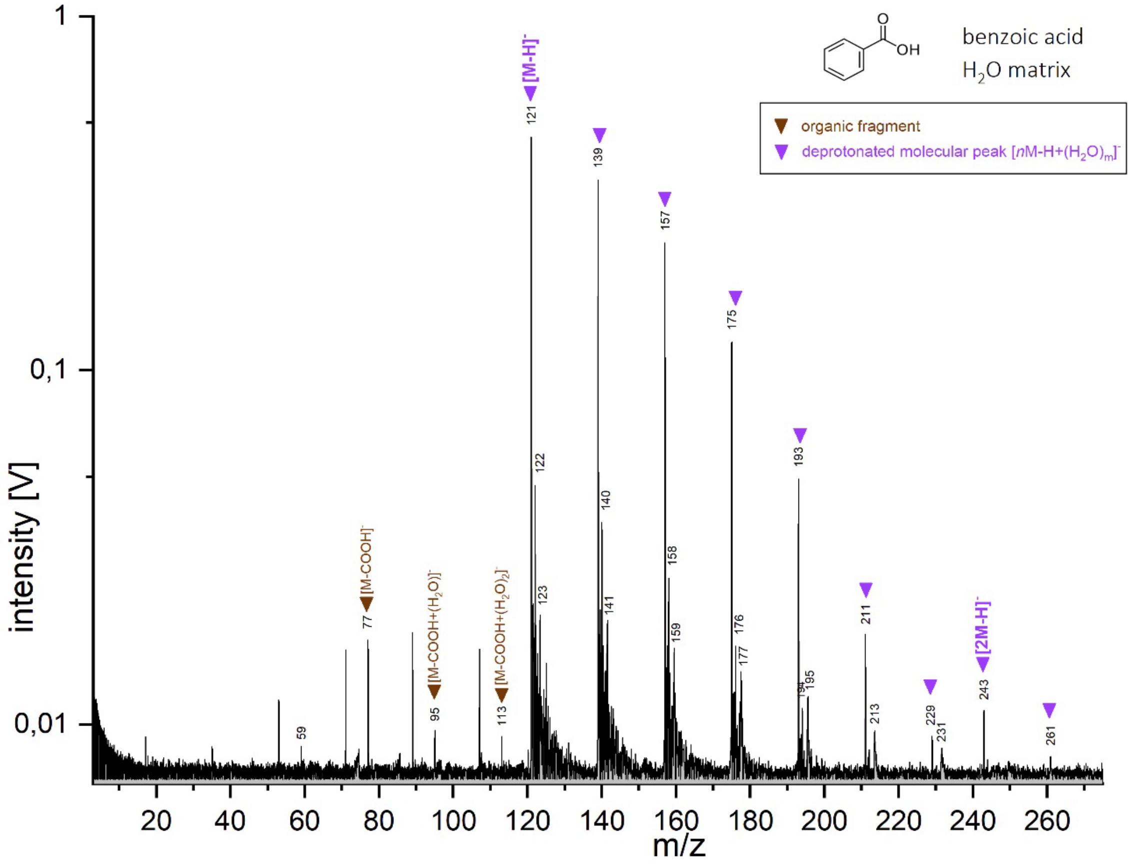

Figure S42. Baseline corrected anion mass spectrum of benzoic acid at a concentration of 0.17wt% in a pure H_2O matrix, recorded at a delay time of 6.3µs. Unlabeled peaks originate exclusively from the water matrix.

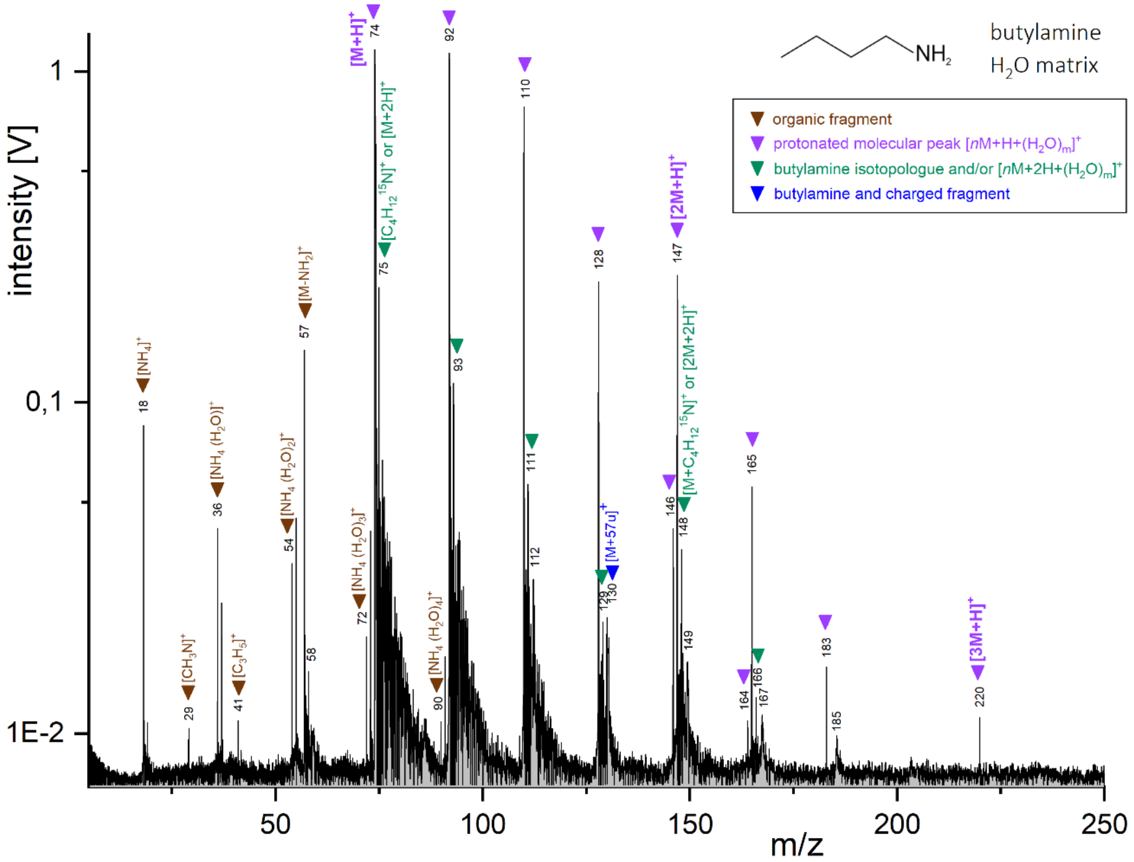

Figure S43. Baseline corrected cation mass spectrum of butylamine at a concentration of 5wt% in a pure H_2O matrix, recorded at a delay time of 6.0µs.

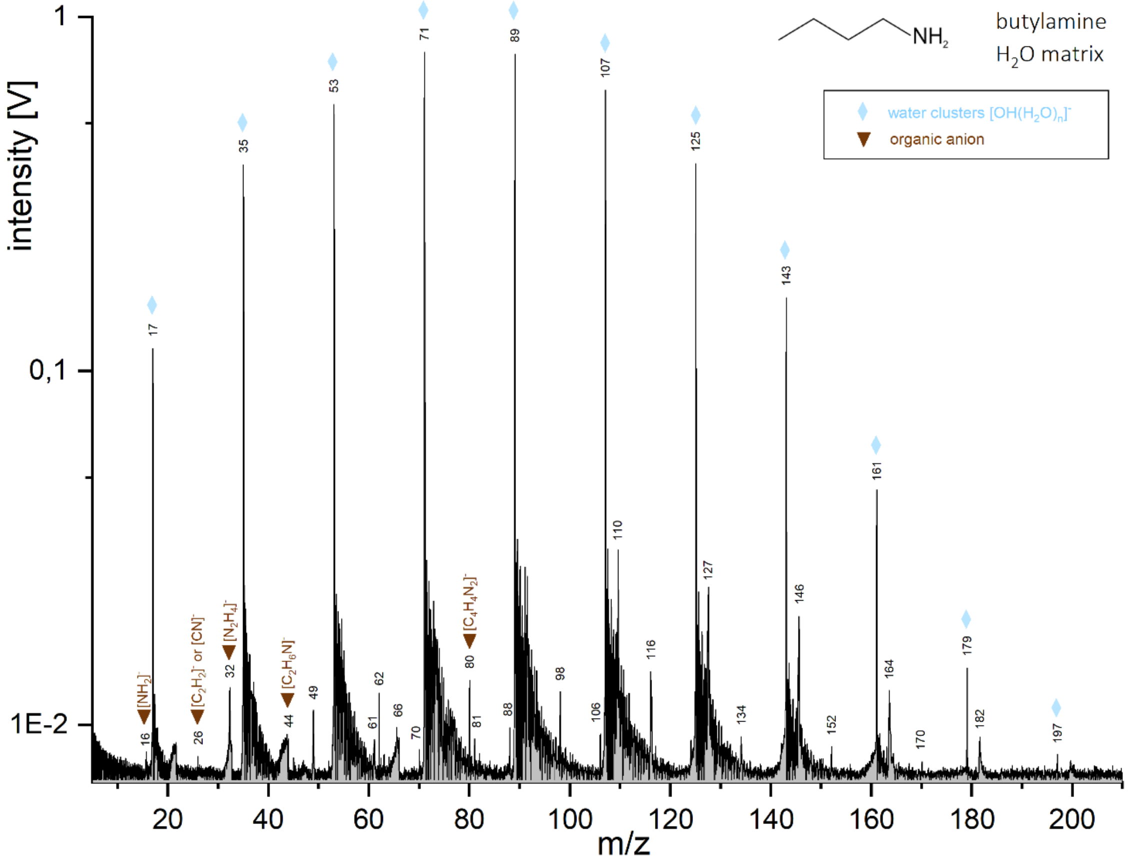

Figure S44. Baseline corrected anion mass spectrum of butylamine at a concentration of 5wt% in a pure H_2O matrix, recorded at a delay time of 6.5µs.

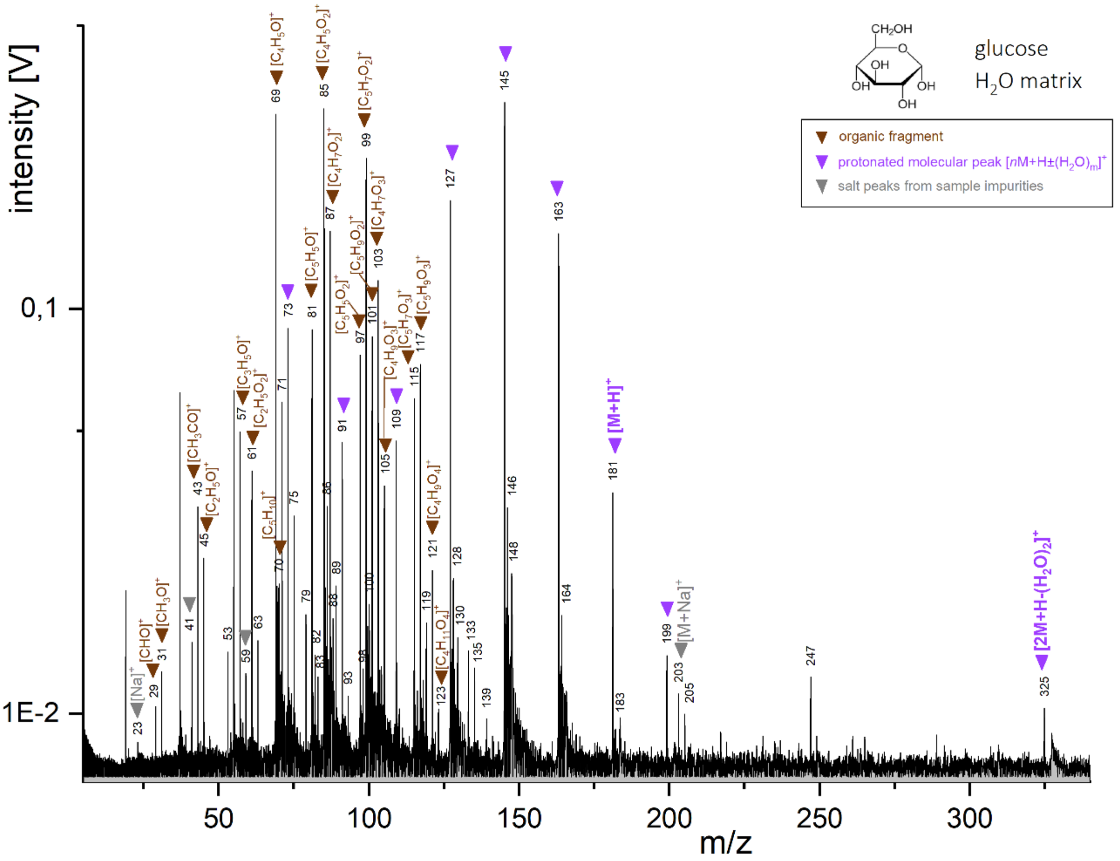

Figure S45. Baseline corrected cation mass spectrum of glucose at a concentration of 5wt% in a H_2O matrix with amberlite®, recorded at a delay time of 5.7µs. Unlabeled peaks originate exclusively from the water matrix.

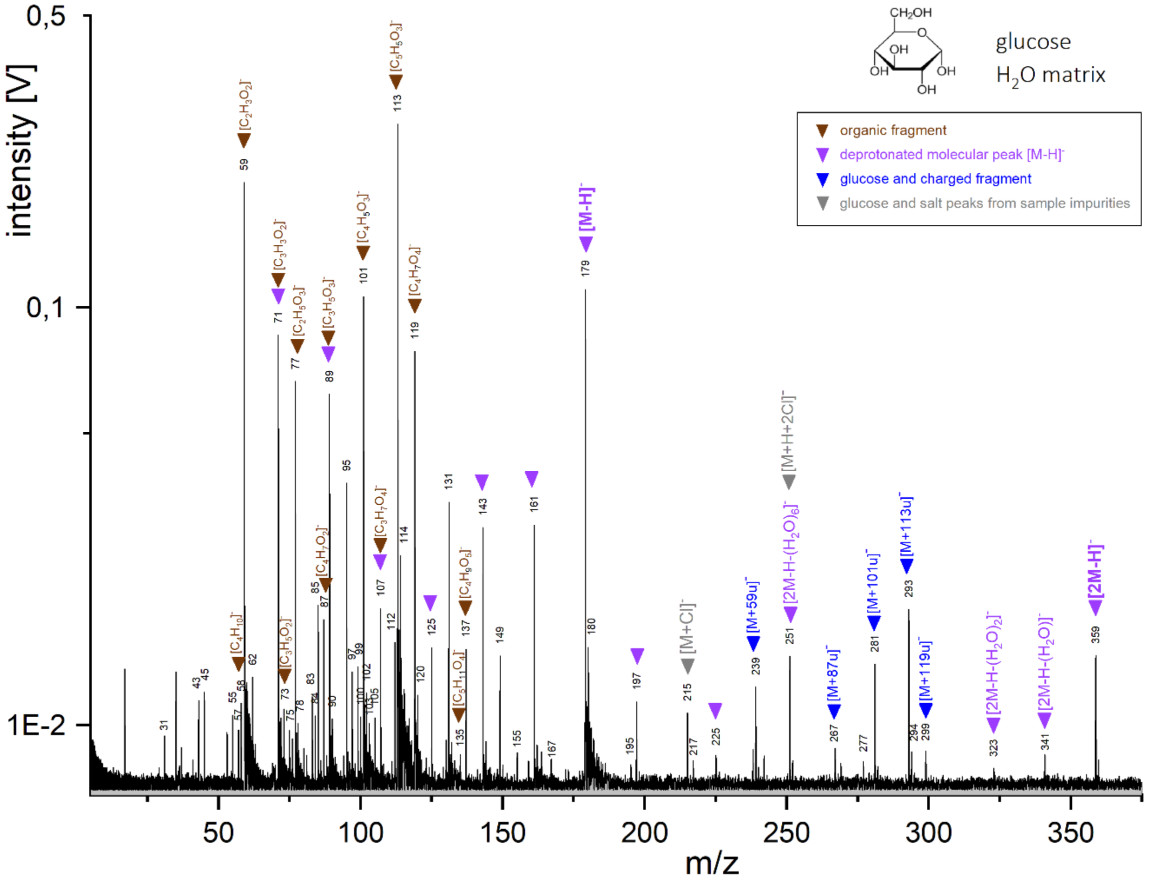

Figure S46. Baseline corrected anion mass spectrum of glucose at a concentration of 5wt% in a pure H_2O matrix, recorded at a delay time of 6.3µs. Unlabeled peaks originate exclusively from the water matrix.

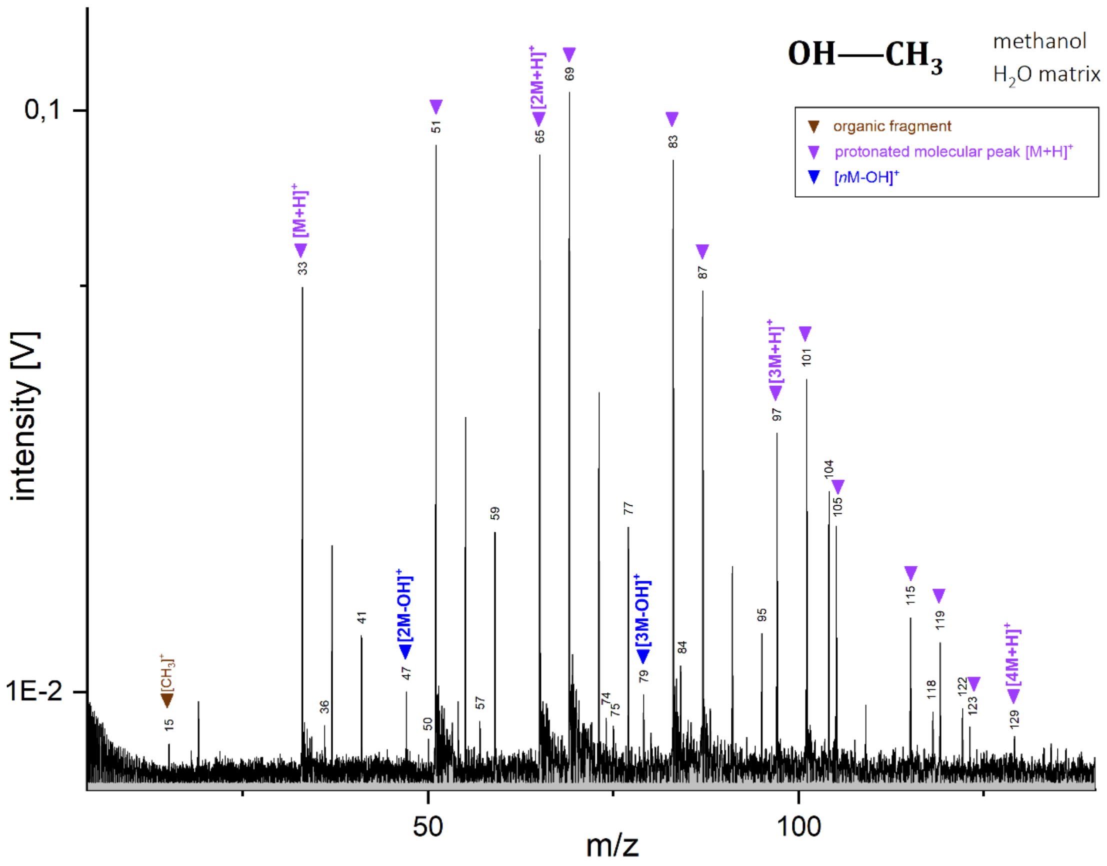

Figure S47. Baseline corrected cation mass spectrum of methanol at a concentration of 5wt% in a pure H_2O matrix, recorded at a delay time of 5.7µs. Unlabeled peaks originate exclusively from the water matrix.

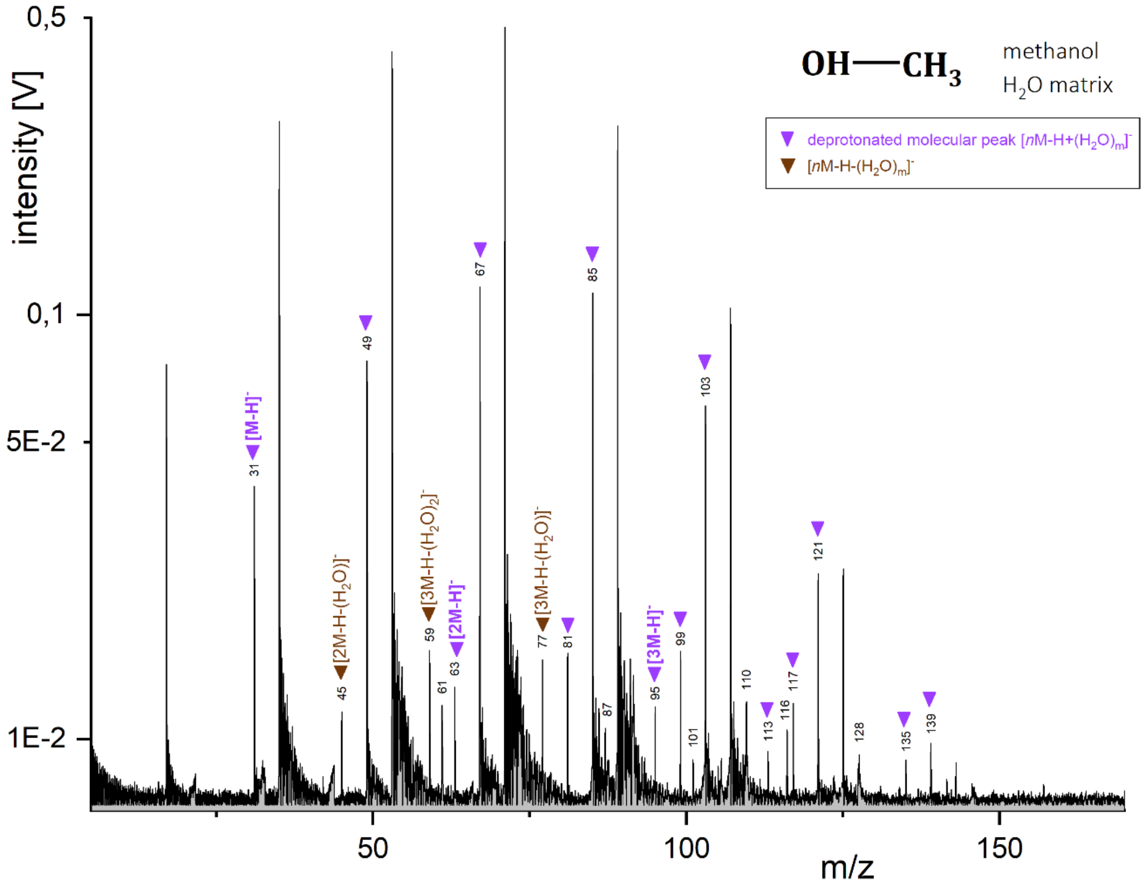

Figure S48. Baseline corrected anion mass spectrum of methanol at a concentration of 5wt% in a pure H_2O matrix, recorded at a delay time of 6.0µs. Unlabeled peaks originate exclusively from the water matrix.

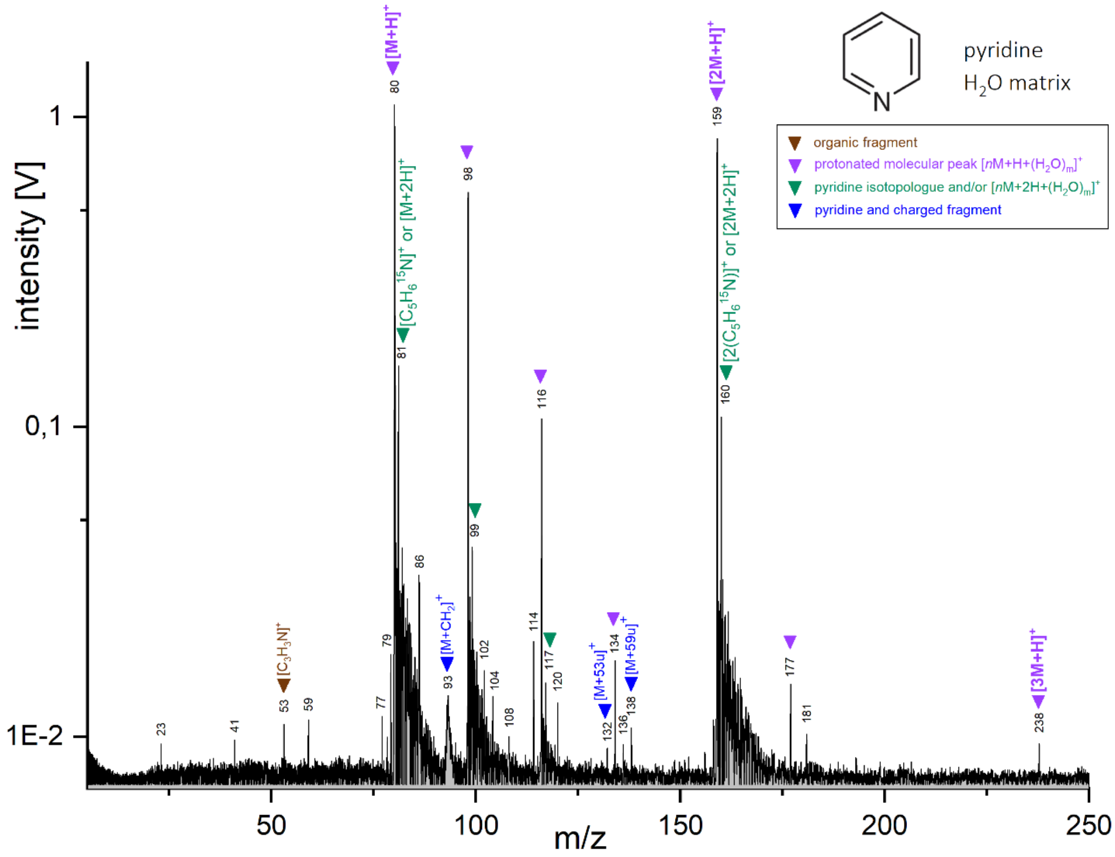

Figure S49. Baseline corrected cation mass spectrum of pyridine at a concentration of 5wt% in a pure H_2O matrix, recorded at a delay time of 6.3µs. Unlabeled peaks originate exclusively from the water matrix.

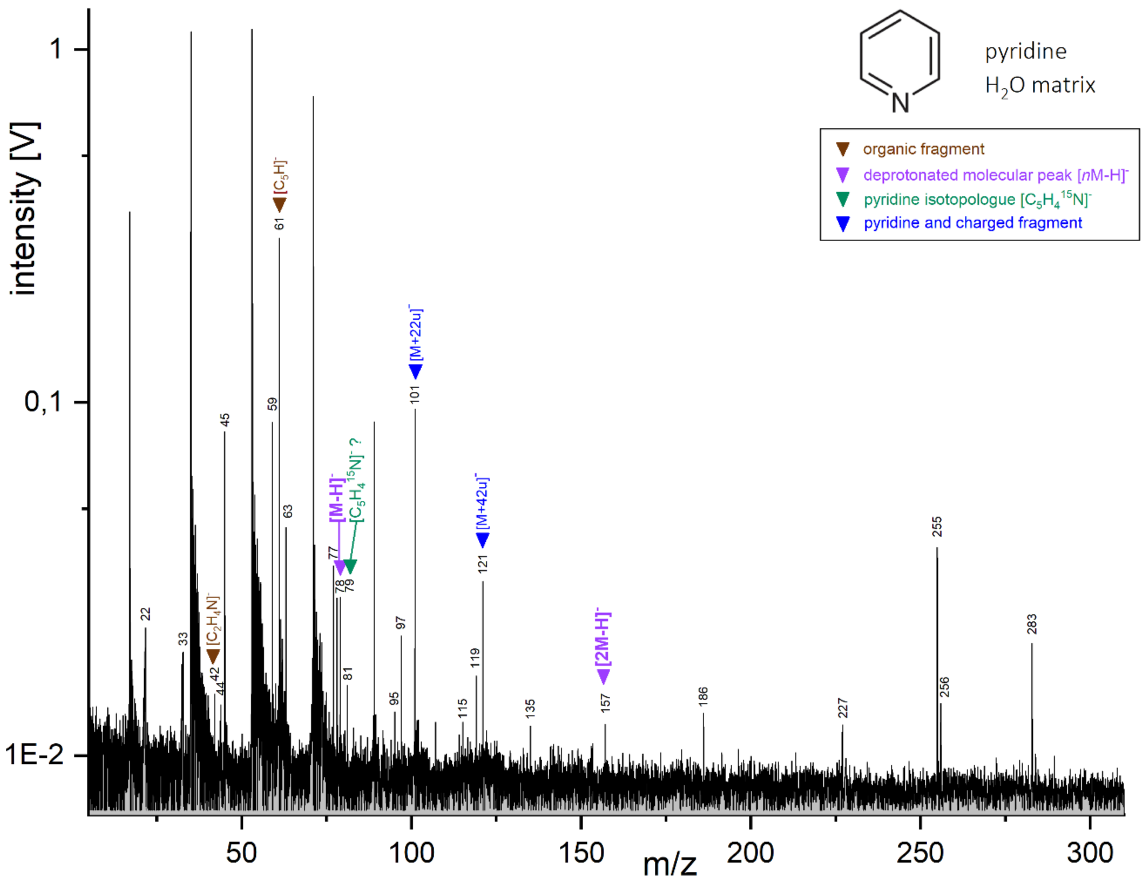

Figure S50. Baseline corrected anion mass spectrum of pyridine at a concentration of 5wt% in a pure H_2O matrix, recorded at a delay time of 6.3µs. Unlabeled peaks originate exclusively from the water matrix.

NaCl concentration	**m/z**	**pure H_2O**	**0.01M**	**0.1M**	**1M**
5-amino-1-pentanol	18	$[NH_4]^+$	$[NH_4]^+$	$[NH_4]^+$	
	30	$[CH_2NH_2]^+$ or $[CH_2O]^+$	$[CH_2NH_2]^+$ or $[CH_2O]^+$	$[CH_2NH_2]^+$ or $[CH_2O]^+$	
	36	$[NH_4 (H_2O)]^+$	$[NH_4 (H_2O)]^+$		
	41	$[C_3H_5]^+$			
	47			UI	UI
	48	$[CH_2NH_2 (H_2O)]^+$	$[CH_2NH_2 (H_2O)]^+$		
	54	UI			
	57	$[M-CH_2O-NH_2]^+$	$[M-CH_2O-NH_2]^+$		
	66	UI			
	69	$[M-OH-NH_3]^+$	$[M-OH-NH_3]^+$	$[M-OH-NH_3]^+$	
	70, 72, 80, 84	UI			
	85	UI	UI	UI	UI
	86	$[M-OH]^+$	$[M-OH]^+$		
	87, 88, 90, 102, 103	UI			
Acetic acid	28			$[CO]^+$	
	42	$[C_3H_6]^+$			
	43	$[M-OH]^+$	$[M-OH]^+$		
	44, 57	UI			
Benzoic acid	23	UI			
	39			$[C_3H_3]^+$	
	41	$[C_3H_5]^+$			
	43, 59, 61, 77	UI			
	79	$[C_6H_7]^+$			
	80	$[C_6H_8]^+$			
	93	$[C_7H_9]^+$			
	95, 104	UI			
	105	$[M-OH]^+$	$[M-OH]^+$		
Butylamine	18	$[NH_4]^+$	$[NH_4]^+$		
	29	$[CH_3N]^+$			
	36	$[NH_4(H_2O)]^+$			
	41	$[C_3H_5]^+$			
	54	$[NH_4(H_2O)_2]^+$			
	57	$[M-NH_2]^+$	$[M-NH_2]^+$		
	58	UI			
	63		UI	UI	
	72	$[NH_4(H_2O)_3]^+$			
Glucose	29	$[CHO]^+$	$[CHO]^+$		$[CHO]^+$
	31	$[CH_2OH]^+$	$[CH_2OH]^+$	$[CH_2OH]^+$	$[CH_2OH]^+$
	43	$[C_2H_3O]^+$	$[C_2H_3O]^+$		$[C_2H_3O]^+$
	45	$[C_2H_5O]^+$	$[C_2H_5O]^+$	$[C_2H_5O]^+$	$[C_2H_5O]^+$
	57	$[C_3H_5O]^+$	$[C_3H_5O]^+$		
	61	$[C_2H_5O_2]^+$	$[C_2H_5O_2]^+$		$[C_2H_5O_2]^+$
	69	$[C_4H_5O]^+$			
	70	$[C_5H_{10}]^+$			
	73	$[C_3H_5O_2]^+$	$[C_3H_5O_2]^+$	$[C_3H_5O_2]^+$	$[C_3H_5O_2]^+$
	75, 79	UI			
	81	$[C_5H_5O]^+$			
	82, 83	UI			
	85	$[C_4H_5O_2]^+$			$[C_4H_5O_2]^+$
	87	$[C_4H_7O_2]^+$			
	88, 89	UI			
	91	$[M+H-(H_2O)_5]^+$			
	93	UI			
	97	$[C_5H_5O_2]^+$			
	99	$[C_5H_7O_2]^+$			

	101	$[C_5H_9O_2]^+$			
	103	$[C_4H_7O_3]^+$			
	105	$[C_4H_9O_3]^+$	$[C_4H_9O_3]^+$	$[C_4H_9O_3]^+$	$[C_4H_9O_3]^+$
	109	$[M+H-(H_2O)_4]^+$			
	115	$[C_5H_7O_3]^+$			
	117	$[C_5H_9O_3]^+$			
	119	UI			
	121	$[C_4H_9O_4]^+$	$[C_4H_9O_4]^+$	$[C_4H_9O_4]^+$	
	123	$[C_4H_{11}O_4]^+$	$[C_4H_{11}O_4]^+$	$[C_4H_{11}O_4]^+$	$[C_4H_{11}O_4]^+$
	127	$[M+H-(H_2O)_3]^+$		$[M+H-(H_2O)_3]^+$	$[M+H-(H_2O)_3]^+$
	128, 130, 133, 135, 139	UI			
	145	$[M+H-(H_2O)_2]^+$			
	146, 148	UI			
	163	$[M-OH]^+$	$[M-OH]^+$	$[M-OH]^+$	$[M-OH]^+$
	164	UI			
	165		UI		
Methanol	15	$[CH_3]^+$			
Pyridine	23, 41	UI			
	53	$[C_3H_3N]^+$			
	59, 77, 79	UI			

Table S1. Fragment peaks, and their respective mass, detected in cation mode for the investigated organics in pure water matrix and at 0.01M, 0.1M and 1M NaCl concentrations, at all investigated delay times and laser power intensities. UI stands for unidentified ion species.

NaCl concentration	**m/z**	**pure H_2O**	**0.01M**	**0.1M**	**1M**
5-amino-1-pentanol	16	$[NH_2]^-$			
	26	$[C_2H_2]^-$ or $[CN]^-$			
	42	$[C_2H_4N]^-$	$[C_2H_4N]^-$		
	43, 44, 45, 46	UI			
	57		UI		
	59	UI	UI		
	60 61, 62, 63, 64, 77, 78, 79, 80, 81, 83	UI			
	86, 88		UI		
	95, 97, 98	UI			
Acetic acid	15	$[CH_3]^-$	$[CH_3]^-$	$[CH_3]^-$	$[CH_3]^-$
	36	UI			
	41	$[M-H_3O]^-$			
	54, 58	UI			
Benzoic acid	59	UI			
	77	$[M-COOH]^-$	$[M-COOH]^-$	$[M-COOH]^-$	$[M-COOH]^-$
	95	$[M-COOH+(H_2O)]^-$			
	113	$[M-COOH+(H_2O)_2]^-$			
Butylamine	16	$[NH_2]^-$			
	26	$[C_2H_2]^-$ or $[CN]^-$		$[C_2H_2]^-$ or $[CN]^-$	
	32	$[N_2H_4]^-$			
	44	$[C_2H_6N]^-$			
	49	UI			
	57		$[M-NH_2]^-$	$[M-NH_2]^-$	
	58			UI	
	61, 62, 66, 70	UI			
Glucose	31	UI			
	43, 45	UI		UI	
	55, 57	UI			
	58	$[C_4H_{10}]^-$	$[C_4H_{10}]^-$	$[C_4H_{10}]^-$	
	59	$[C_2H_3O_2]^-$	$[C_2H_3O_2]^-$	$[C_2H_3O_2]^-$	
	62	UI			
	71	$[C_3H_3O_2]^-$ or $[M-H-(H_2O)_6]^-$	$[C_3H_3O_2]^-$ or $[M-H-(H_2O)_6]^-$	$[C_3H_3O_2]^-$ or $[M-H-(H_2O)_6]^-$	
	73	$[C_3H_5O_2]^-$			
	75	UI			
	77	$[C_2H_5O_3]^-$	$[C_2H_5O_3]^-$		
	78, 83, 84, 85	UI			
	87	$[C_4H_7O_2]^-$	$[C_4H_7O_2]^-$	$[C_4H_7O_2]^-$	
	89	$[C_3H_5O_3]^-$ or $[M-H-(H_2O)_5]^-$	$[C_3H_5O_3]^-$ or $[M-H-(H_2O)_5]^-$	$[C_3H_5O_3]^-$ or $[M-H-(H_2O)_5]^-$	
	90, 95, 97, 99, 100	UI			
	101	$[C_4H_5O_3]^-$	$[C_4H_5O_3]^-$	$[C_4H_5O_3]^-$	
	102, 103, 105	UI			
	107	$[C_3H_7O_4]^-$ or $[M-H-(H_2O)_4]^-$	$[C_3H_7O_4]^-$ or $[M-H-(H_2O)_4]^-$	$[C_3H_7O_4]^-$ or $[M-H-(H_2O)_4]^-$	
	112	UI			
	113	$[C_5H_5O_3]^-$			

	114	UI		
	116			UI
	117		$[C_5H_9O_3]^-$	$[C_5H_9O_3]^-$
	119	$[C_4H_7O_4]^-$	$[C_4H_7O_4]^-$	$[C_4H_7O_4]^-$
	120	UI		
	125	$[M-H-(H_2O)_3]^-$	$[M-H-(H_2O)_3]^-$	$[M-H-(H_2O)_3]^-$
	131	UI		
	135	$[C_5H_{11}O_4]^-$	$[C_5H_{11}O_4]^-$	
	137	$[C_4H_9O_5]^-$	$[C_4H_9O_5]^-$	
	143	$[M-H-(H_2O)_2]^-$	$[M-H-(H_2O)_2]^-$	$[M-H-(H_2O)_2]^-$
	149, 155	UI		
	159		UI	UI
	161	$[M-H-(H_2O)]^-$	$[M-H-(H_2O)]^-$	$[M-H-(H_2O)]^-$
	167	UI		
	171		UI	
Methanol				
Pyridine	22, 33	UI		
	42	$[C_2H_4N]^-$		
	44, 45, 59	UI		
	61	$[C_5H]^-$		
	63, 77	UI		

Table S2. Fragment peaks, and their respected mass, detected in anion mode for the investigated organics at 0.01M, 0.1M and 1M NaCl concentrations, at all investigated delay times and laser power intensities. UI stands for unidentified ion species.